BIOMEDICAL ENGINEERING MSc PROGRAM
UNIVERSITY OF CRETE
TECHNICAL UNIVERSITY OF CRETE
FOUNDATION FOR RESEARCH AND TECHNOLOGY-HELLAS

Research Grade Thesis

Title:
"Polymeric drug carrier for ocular drug delivery"

Student's Name: Fergadis Georgios Dimitrios
Supervisor's Name: Prof. Maria Vamvakaki

2nd member committee name: Prof. Miltiadis Tsilimbaris
3rd member committee name: Prof. Ioannis Charalampopoulos

Heraklion October 2022

Acknowledgements

First of all, I would like thank my supervisor Professor Maria Vamvakaki for accepting me as a master's student in her lab and guiding me through the whole process. Also, I would like thank Professor Miltiadis Tsilimbaris and Professor Ioannis Charalampopoulos for accepting my invitation and participate in my evaluation committee. Next, I would like thank and express my gratitude to the PhD candidate Ms Maria Psarrou, who helped me throughout the process by giving me advices, supporting me, evaluating my progress and being extremely patient with me. In addition, I couldn't leave out my colleagues of the Synthetic Chemistry lab for all the help and support they gave me over the whole duration of this work. They were the best colleagues anyone could have. A big thank you goes to my friends outside the lab who helped me and supported me all the way.

Last but not least, I would like to thank my parents, Stamatis and Eleni as well as my brother Fotis, for all the help and support I received throughout the years, from my undergraduate studies to my master's degree, and for providing me with all the essentials all the way through my life. I really could not thank them enough.

Abstract

The presence of many dynamic and static obstacles in the ocular tissues, such as the blood-ocular barrier, tear production, and the cornea's limited permeability, renders the effective ocular drug delivery a challenging task. Polymeric micelles, liposomes, hydrogels, polymer-drug, and protein-drug conjugates are examples of the modalities developed and tested, throughout the years, for ocular drug delivery [1]. However, to the best of our knowledge, there are no reports on biodegradable systems, which include FDA-approved materials, that are also capable of slowing down the drug release profiles, documented in the literature so far. As a result, the development of drug delivery systems that can maintain an appropriate drug concentration in various ocular tissues for an extended period of time is of great importance. In the present thesis, we have developed polymeric nanocarriers for the encapsulation and delivery of Flurbiprofen, a nonsteroidal anti-inflammatory drug, used in ocular therapy. Next, hydrogels comprising a oxidized, natural polysaccharide, dextran, were used as a matrix to incorporate these nanocarriers, as it has been shown that hydrogels can prolong the release of the drug molecules into the medium [2].

In the first part of this thesis, amphiphilic poly(ethylene glycol)-*block*-poly(L-lactide) (PEG-*b*-PLLA) diblock and PLLA-*b*-PEG-*b*-PLLA triblock copolymers were synthesized. For the synthesis of the diblock and triblock copolymers, ring-opening polymerization of the hydrophobic monomer, L-lactide, was carried out using monohydroxy and dihydroxy PEG as the macroinitiator, respectively [3]. Size exclusion chromatography (SEC) was employed to confirm the successful synthesis of the copolymers and proton nuclear magnetic resonance (^{1}H NMR) spectroscopy was used to ascertain their composition. Next, the amphiphilic copolymers were self-assembled into micellar structures in water, which entrapped small hydrophobic drug molecules within their micellar cores [4]. Micelles were prepared from both the diblock and triblock copolymers, as well as from a mixture of the two copolymers in order to form more complex structures. Dynamic light scattering (DLS) was used to determine the hydrodynamic size of the nanocarriers. Transmission electron microscopy (TEM) and scanning electron microscopy (SEM) were employed to confirm the morphology of the nanocarriers. Next, the release profile of flurbiprofen

from the polymeric nanostructures was studied. All the micellar structures released the drug within 4 days reaching 100% of release. Thus, the different chemical composition of the copolymers was not able to slow down sufficiently the release kinetics of the drug.

In the second part of this work, to further slow-down the release profile of flurbiprofen from the polymer carriers, we developed biodegradable hydrogels and incorporated the drug loaded micellar structures within their porous structures. The hydrogels were prepared through the reaction of oxidized dextran (Ald-Dex), which bears aldehyde groups, with adipic acid dihydrazide (AAD), to form acylhydrazone bonds. The crosslinker, adipic acid dihydrazide, ranged between 10 and 30 wt% with respect to the polymer. The synthesized hydrogels were characterized in terms of their chemical composition and morphology by Fourier Transform infrared spectroscopy (FTIR) and SEM, respectively. Next, the flurbiprofen loaded polymeric nanocarriers were incorporated within the hydrogels and the release profile of the drug molecules was studied. The hydrogels were found to release 100% of the payload within 7 days, exhibiting a delay in the drug release profile compared to the micellar system alone.

Table of contents

Chapter 1: Introduction

1.1 Drug delivery

The term drug delivery refers to the methods of transporting a pharmaceutical compound inside the human body to achieve a therapeutic effect. Different ways of administrating drugs include oral, transnasal or rectal administration. Injections are also widely used in medicine to deliver drugs, the most common being intravenous and subcutaneous injections. The methods of drug administration are constantly evolving in order to increase their efficacy. All of the previous methods are characterized by a relatively fast release of the substance(s), and thus have limited patient compliance. Current research focuses on developing drug delivery systems that can sustain the release of the pharmaceutical product, prolonging its activity in the body, thus decreasing the frequency of administration [5]. These systems have the ability to actively control the rate, as well as the site of the release of the drug [5]. Numerous studies have been carried out in an effort to target particular organs or cells in the body in order to regulate the release of pharmaceutical substances [6], [7]. For the sustained and targeted administration of therapeutic drugs, nanocarriers such liposomes, nanoparticles, and micelles have been utilized [8], [9].

1.2 Ocular drug delivery

Due to the unique anatomical and physiological barriers that exist in the eye, scientists have faced significant difficulties in developing effective ocular drug delivery systems. These barriers include the tear film, the aqueous humor as well as the sclera, choroid and vitreous body and cause rapid drug removal or poor drug absorption from the eye, requiring frequent dose administration. Both invasive and non-invasive procedures are used to treat the eye problems (**Fig. 1.1**). Invasive treatments, like intraocular injections, surgery and laser therapy, are usually accompanied by complications, such as inflammation, high intraocular pressure, retinal hemorrhage and potential visual loss. Oral drugs, eye ointments, and topical eye drops are examples of non-invasive therapy. Although these techniques have been used extensively to treat a variety of pathologies, their limited clinical applicability stems

from their sort life-time in the eye [7]. Advancements in nanotechnology pave the way for the incorporation of new drug delivery systems such as contact lenses, microneedles and implants.

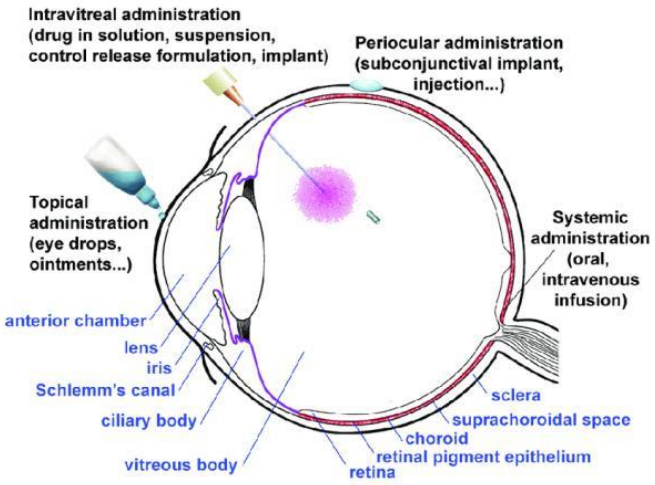

Fig. 1.1: The anatomy of the eye and various routes of drug administration [10]**.**

1.2.1 Contact lenses

Contact lenses are curved plastic disks that fit over the cornea. After being applied, the contact lens attaches to the tear film covering the cornea due to surface tension. For the ocular delivery of many medications, including blockers, antihistamines, and antimicrobials, drug-loaded contact lenses have been developed. It is hypothesized that in the presence of contact lenses, drug molecules have a longer residence period in the post-lens tear film, resulting in higher drug flow across the cornea and less drug influx into the nasolacrimal duct [11]. Different types of drug-loaded contact lenses have been developed, for instance lenses soaked in drug solutions, lenses with drug-loaded particles embedded in the lens and molecular imprinted contact lenses. All of the previous mentioned approaches exhibit an increase in the drug's bioavailability in the eye [12]–[14].

1.2.2 Ocular implants

Intraocular implants are specifically developed to offer localized controlled drug release over an extended period of time. These implants are placed intravitreally and they can be non-biodegradable and biodegradable. The non-biodegradable systems are usually made from polymers such as polyvinyl alcohol (PVA) and they need to be surgically removed after a certain time. Commercial systems include Vitrasert® and Retisert® which are both FDA approved. They are capable of a sustained release of a pharmaceutical product for an extended period of months to years [11]. However, these devices present certain side effects like, endophthalmitis, vitreous haze, hemorrhage or even cataract development. Biodegradable implants are made of polymers like poly(lactic acid) (PLA) and poly(lactic acid-*co*-glycolic acid) (PLGA) and they are capable of a sustained drug release for a period of up to 6 months [15]. Some examples of available products are Surodex™ and Ozurdex®.

1.2.3 Microneedles

Using a microneedle-based approach, drugs can be delivered to the posterior tissues of the eyes in a minimally invasive manner. The danger and side effects of intravitreal injections, such as retinal detachment, hemorrhage, cataract and endophthalmitis may be lessened by using this microneedle-based administration approach. Additionally, this approach might support the delivery of therapeutic drug concentrations to the retina and choroid by avoiding the blood-retinal barrier. The needles aid in the deposit of a drug or carrier system into the sclera or into the suprachoroidal region, a small gap between the sclera and choroid. Drug diffusion into deeper ocular tissues, the choroid, and the neuronal retina may be facilitated by this approach [16]. In order to prevent harm of the deeper ocular tissues, microneedles are specifically made to only pierce the sclera by hundreds of microns. These needles have been studied and they may be promising for a safe and targeted way of delivering drugs to the sclera tissues [17].

1.3 Types of drug nanocarriers

Since 1960, various nanocarriers have been extensively studied for the delivery of drugs. Structures with dimensions between 1 and 1000 nm are known as nanoparticles (NPs). These particles should not be larger than 10 μm in order to prevent a feeling of a foreign body following administration [18]. NPs made of biodegradable polymers are potential candidates for use as medication carriers to alleviate the problem of frequent injections. The drug's half-life can be extended by the NPs by shielding it from the bloodstream proteins. They may also decrease the need for repeated doses by slowing the drugs' release profile. Among the most frequently studied systems are vesicles, polymer-drug conjugates, polymeric micelles, and liposomes (**Fig. 1.2**).

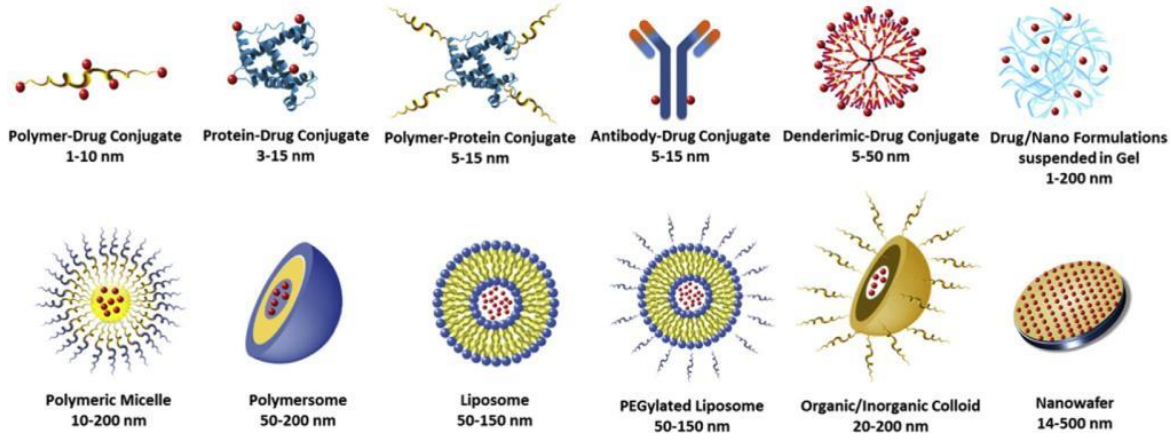

Fig. 1.2: Schematic depiction of the most common nanomedicine formulations used in ocular delivery [1].

1.3.1 Liposomes

Liposomes are "bubble-like" structures that have a phospholipid bilayer which is analogous to a cell membrane. These structures are capable of encapsulating small molecules, such as hydrophilic or lipophilic drugs. Liposomes are the most common and well-studied drug delivery vehicles. Additionally, poly(ethylene glycol) (PEG) chains may be affixed to the liposomes' bilayer to extend their lifetime within the bloodstream. According to research by *Karn et al.*, liposomes containing cyclosporine A , a drug used to treat dry eye syndrome, are less irritating to the eye and more effective than store-bought products [19].

1.3.2 Polymeric nanoparticles

In comparison to liposomes, polymeric NPs have a variety of benefits, including enhanced stability and the ability to support prolonged drug release. A copolymer made of poly(lactic acid) and poly(glycolic acid) called poly(lactic acid-*co*-glycolic acid) (PLGA) is often used in biomedical applications such as surgical sutures, tissue engineering scaffolds, and drug delivery systems [20]. PLGA is a biodegradable, FDA approved polymer whose mechanical properties can be modified by varying the PLA/PGA mole ration. PLGA NPs have the ability to encapsulate a range of drugs and can target particular cells or parts of the body [21], [22]. *Cañadas et al* examined the effectiveness of PLGA nanoparticles as a pranoprofen delivery system inside the cornea [23]. Nanoparticles encapsulating pranoprofen had a rapid anti-inflammatory effect and a lengthy retention time on the cornea's surface, lowering ocular edema significantly. Another case is nanoparticles made of chitosan. Deacetylating the chitin found in crab shells yields the polymer known as chitosan. It contains N-acetylglucosamine and glucosamine. Because of its mucoadhesive characteristics, chitosan has a high penetration of the ocular surface in ophthalmic drug administration [24]. The use of chitosan-based NPs for ocular medication delivery has been investigated in the past [25], [26].

1.3.3 Polymeric micelles

Amphiphilic molecules can self-assemble into spherical structures, called micelles, in a suitable solvent. Hydrophobic interactions cause amphiphilic molecules to self-assemble in an aqueous environment at a particular concentration, known as the critical micelle concentration (CMC) (**Fig.1.3**). The term "CMC" refers to the minimal molecule concentration necessary for the formation of micelles. These structures are typically in the nanometer range and feature a hydrophobic core and a hydrophilic shell [27]. Amphiphilic diblock copolymers can self-assemble into polymeric micelles, with the hydrophilic chains expanding in water to form the micelles' corona or shell and the hydrophobic blocks forming the inner core [4].

Among the most widely studied biodegradable block copolymers that can self-assemble into polymer micelles are poly(ethylene glycol)-*b*-poly(propylene glycol) (PEG-PPG), poly(ethylene glycol)-*b*-poly(-caprolactone) (PEG-PCL), and poly(ethylene glycol)-*b*-poly(L-lactide) (PEG-PLLA) [19], [20], [28]–[31]. PLLA is synthetic hydrophobic polyester produced from the polymerization of L-lactide. When this polyester is copolymerized with PEG, it leads to the production of an amphiphilic copolymer [32]. PEG is an excellent candidate for the synthesis of a biodegradable polyester due to its hydrophilic and biocompatible nature [3], [33]. In an aqueous solution, polymeric chains can self-assemble into micellar nanostructures. These micelles are constructed of the hydrophobic PLLA blocks in the core and the hydrophilic PEG blocks in the shell. The shell stabilizes the micelles in the medium, whereas the core can act as a reservoir for hydrophobic drugs [6]. PEG-PLLA diblock and triblock copolymers have been investigated for use in drug delivery and tissue engineering [6], [34], [35].

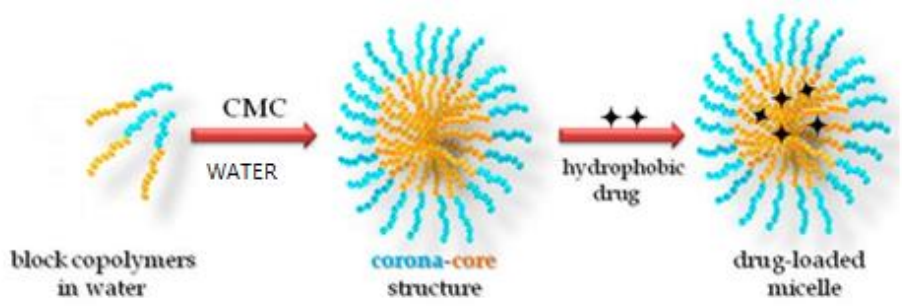

Fig. 1.3: Schematic illustration of the micellization process of diblock copolymers and the encapsulation of drug molecules [4]**.**

There are many different methods for the production of polymer micelles, for example the non-selective dissolution method, the thin-film method as well as the dialysis technique. In the non-selective-selective solvent method, the copolymer is dissolved in a common solvent for both blocks before being mixed with water to serve as a selective solvent. Using this method, micelles with uniform sizes and low polydispersity are formed. In the second method, the polymer is dissolved in an organic solvent and then evaporated to produce a polymer film. After the film has been hydrated using an aqueous solvent, the polymer nanostructures are formed. Finally, in the dialysis approach, the copolymer is dissolved in the good solvent for

both blocks and is then placed in a dialysis bag. The bag is placed in aqueous media, usually for a period of 24h. The gradual inflow of the solvent molecules into the dialysis bag drives the self-assembly of the polymeric chains due to hydrophobic interactions.

1.3.3.1 Characteristics of the micelle morphology

The micelles' shell is made up of the hydrophilic blocks of the amphiphilic copolymers. The charge, lipophilicity, and size of the micelles are all determined by the shell of the micellar structure. These variables significantly affect the biological characteristics of the carrier, including blood circulation time, pharmacokinetics, and biocompatibility [36]. Several factors affect the micellar morphology. The most significant factors are the aggregation number, packing parameter, and CMC. The hydrophobic interactions between the hydrophobic building units of the copolymer and the solvent promote micelle formation in aqueous solutions. The formation of micelles is facilitated and more stable micelles are produced, as the hydrophobicity is increased [37]. The hydrophobic and hydrophilic ratio, as well as the interaction between the polymer and the solvent, which can be influenced by factors such as the solution temperature and pH, are essentially determining the CMC. The most significant factor in determining the morphology of the micelles is the packing parameter. The packing parameter is defined as follows:

$$p = \frac{v}{a_0 * l_c}$$

where a_0 is the hydrophilic group's contact area, and l_c, v are the length and volume of the hydrophobic block, respectively. Spherical micelles are created for $p<1/3$, cylinders are formed for $1/3<p>1/2$, and vesicles are formed for $½>p$ [38].

A micelle comprises a certain number of polymer chains, known as the aggregation number. The length of the copolymer chain and the proportion of hydrophobic to hydrophilic segments have a significant impact on the aggregation number [39].

1.4 Mechanisms of drug release from polymeric micelles

Drug release is the flow of a drug molecule from the polymeric micelle to its exterior and into the surrounding environment [40]. **Fig. 1.4** depicts the three main drug release mechanisms: polymer degradation, passive diffusion of the drug molecules that have been encapsulated, and a combination of the two [41]. In the first mechanism, the degradation of the polymeric chains causes the micelles to destabilize, allowing the medication to escape **(Fig.1.4a**). As seen in **Fig.1.4b**, in the second mechanism the drug molecules simply diffuse through the micelle and into the surrounding environment. Finally, for the last mechanism we can observe the active release driven by a combination of polymer degradation and diffusion in **Fig. 1.4c**. Phase 1 of the drug release mechanism is characterized by the rapid diffusion of the drug molecules into the medium as a result of drug absorption onto the surface of the nanocarriers. This phase is known as the burst release phase. The characteristics of the polymeric system govern the phase 2 (controlled release phase) process. Diffusion is the main process when the rate of drug diffusion is higher than the rate of polymer degradation; otherwise, polymer degradation drives drug release [42].

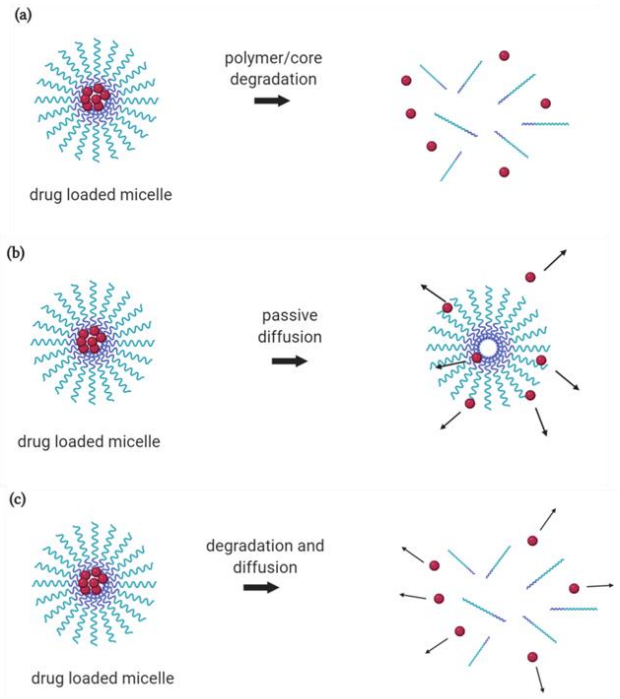

Fig. 1.4: Release mechanisms of drug molecules from micellar structures by a) degradation of the polymeric chains, b) diffusion of the drug molecules c) a combination of degradation and diffusion. Created with BioRender.com

1.4.1 Factors affecting drug release

Several factors can affect the drug release rate from polymeric micelles. The size of the micelles increases with the polymer molecular weight, slowing down the rate of release. The release of the drug molecules is significantly influenced by the length of the hydrophilic and hydrophobic blocks in the copolymer. The capability for drug loading increases with the micelle size (longer hydrophobic chains) [30]. According to *Yang et al*, high molecular weight PLA copolymers form tightly packed micelles as a result of hydrophobic interactions between the drug molecules and the PLA chains, which delays the rate at which the drug is released from the micelles [43].

Finally, the micelle formation process can affect the size, shape, drug loading capacity, stability, rate and degree of drug release of the nanocarriers [44]. Additionally, important factors in drug release include the solvent, the pH of the solution, and the copolymer content [45].

1.5 Ring Opening Polymerization (ROP)

According to IUPAC, ring opening polymerization is a process used to polymerize cyclic monomers and create acyclic polymers or polymers with fewer cycles [46]. An acyclic chain is generated when a reactive center attacks a cyclic monomer, starting the polymerization of the monomer. **Fig.1.5** illustrates the general scheme of ring-opening polymerization.

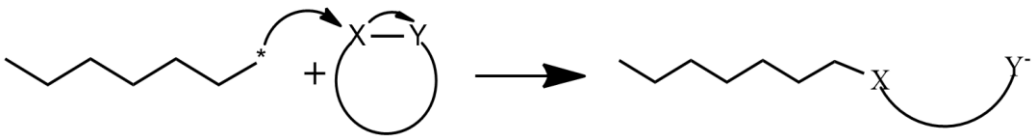

Fig. 1.5: General scheme of ROP. The * refers to an anionic, cationic or radical center.

This method has a variety of advantages, one of which is its ability to create high molecular weight polymers with a controlled polydispersity index (PDI) [47]. Catalysts are required for ROP to proceed. The most commonly employed metal-

complex is stannous octoate (Sn(Oct)2) or tin(II) 2-ethylhexanoate. However, metal complexes can leave residues that can compromise the polymer's use in the biomedical field [48]. To overcome this problem, new organocatalysts have been developed and are widely used for the catalysis of ROP, such as 1,8-diazabicycloundec-7-ene (DBU), 1,4,7-triazabicyclodecene (TBD) and 4-Dimethylaminopyridine (DMAP) [49].

1.6 Flurbiprofen

Flurbiprofen (2-(3-fluoro-4-phenylphenyl) propanoic acid), a propionic acid derivative, is an antipyretic and analgesic nonsteroidal anti-inflammatory drug (NSAID) (**Fig.1.6.**). oral formulations of flurbiprofen can be used to treat the symptoms of rheumatoid arthritis, osteoarthritis, and anklylosing spondylitis. Prior to eye surgery, flurbiprofen may also be used topically to avoid or alleviate intraoperative miosis. Flurbiprofen is structurally and pharmacologically related to fenoprofen, ibuprofen, and ketoprofen.

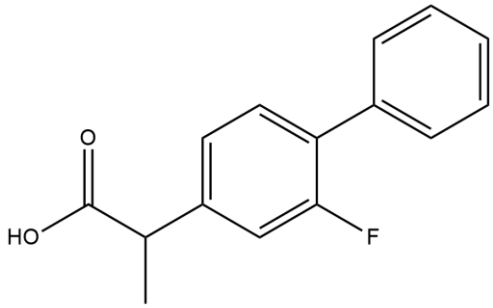

Fig.1.6: Structure of Flurbiprofen

1.7 Hydrogels

A hydrogel is a three-dimensional structure, capable of swelling in water, while preserving its form. The presence of hydrophilic groups such as $–NH_2$, -COOH, -OH, $-CONH_2$, -CONH-, and $-SO_3H$ contributes to the network's hydrophilicity and swelling ability in aqueous media [50]. The ability of hydrogels to swell under biologically relevant conditions makes them an excellent class of materials for biomedical applications such as drug delivery and tissue engineering [51]–[54]. Polymer hydrogels are produced by cross-linking the polymer chains either through physical or chemical cross-links. Physical hydrogels are formed through non-covalent bonds such as hydrogen bonds, hydrophobic or crystalline interactions and chain entanglements and the process is usually reversible. Chemical hydrogels are cross-linked via covalent bonds, which provide the gel with mechanical stability. Polymer hydrogels can be divided according to the source of the polymer, into natural or synthetic polymer hydrogels. Other ways of classification can be seen in **Fig.1.7.**

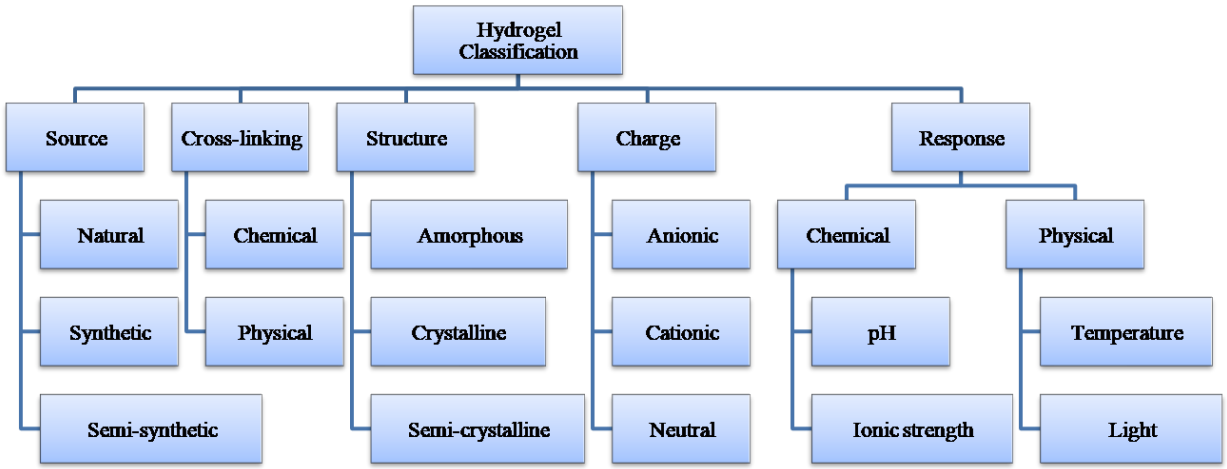

Fig.1.7: Classification of hydrogels based on their different properties.

Chemically cross-linked polymer hydrogels are formed by adding a small molecule, known as crosslinker, to the polymer chains and linking them through covalent interactions. By controlling the degree of cross-linking, the characteristics of the material can be altered, such as the swelling ability, the porosity of the gel, the

elasticity of the hydrogel, etc. that can highly influence the properties of the cross-linked network, including the release rate of the loaded drug molecules [55]. The valuable feature of hydrogels in drug delivery studies is their ability to release pharmaceuticals over extended periods of time (sustained release), which allows for the delivery of a high concentration of an active pharmaceutical ingredient to a specific region [56]. Some of the most commonly used hydrogels are formed from synthetic polymers, such PEG, PVA, or poly(2-hydroxyethyl methacrylate) (PHEMA), or from naturally occurring polymers, such as agarose, alginate, chitosan, collagen, fibrin, and hyaluronan [13], [57]–[61].

1.7.1 Dextran-based hydrogels

Dextran is a member of the polysaccharide family, which is formed by poly-α-D-glycosides, and is synthesized by a variety of bacteria. The main feature of this polymer is the presence of α-1,6 glycosidic bonds. Its molecular weight can vary between 3 and 2000 kDa [62]. The chemical structure of the polymer can be seen in **Fig. 1.8.**

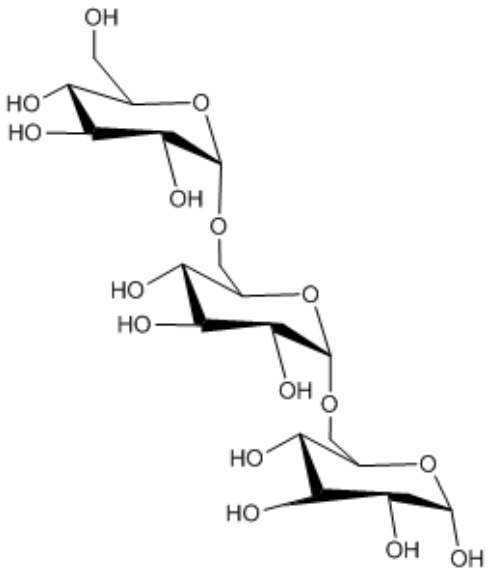

Fig. 1.8: Chemical structure of dextran.

Due to its high water solubility and linear structure, dextran has been mainly employed in the biomedical field as a plasma volume expander [63]. In addition, the polysaccharide is stable in mild acid and basic conditions and its high amount of hydroxyl groups makes it a perfect candidate for various modifications reacrtions. Undoubtedly, the most common is the oxidation of dextran with sodium periodate to generate aldehyde groups. These reactive groups can then be used to produce a hydrogel based on the Schiff base reaction [64].

The dextran oxidation involves the attack of vicinal diols of the pyranose ring, resulting in the cleavage of the C-C bond, particularly the C_3-C_4 bond, to yield aldehyde groups (**Fig.1.9**). Depending on the molar ratio between dextran and sodium periodate, different oxidation degrees can be achieved which alter the polymer characteristics [65].

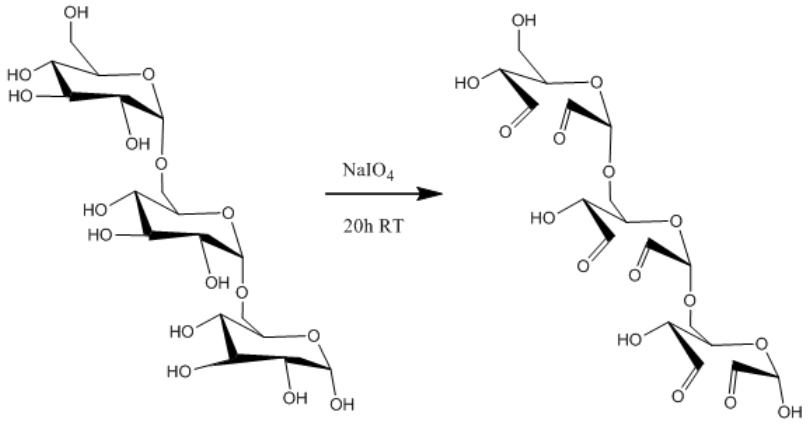

Fig.1.9: Oxidation of dextran in the presence of sodium periodate.

For low oxidation degrees, the aldehyde groups may not be detectable by spectroscopic techniques due to the reaction of the aldehyde groups with neighboring hydroxyl groups and the formation of hemiacetals [66]. These side reactions can influence the final degree of oxidation and the reactivity of the polymer for hydrogel formation [65].

Hydrogels made by cross-linking dextran polymer chains are based on the Schiff base reaction. The reaction involves the formation of covalent imine bonds between an amine and an aldehyde or ketone group. The general structure of the Schiff base bond is illustrated in **Fig. 1.10**.

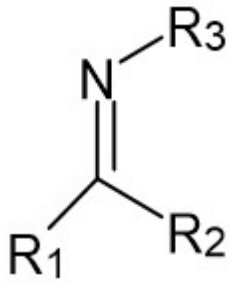

Fig. 1.10: Schematic illustration of the imine (Schiff base) bond

The most common hydrogels obtained via this approach are based on the reaction of aldehydes or ketones with primary amines, hydrazides and acylhydrazides or aminooxy groups and the formation of imines, hydrazones or acylhydrazones and oximes, as shown in **Fig. 1.11**.

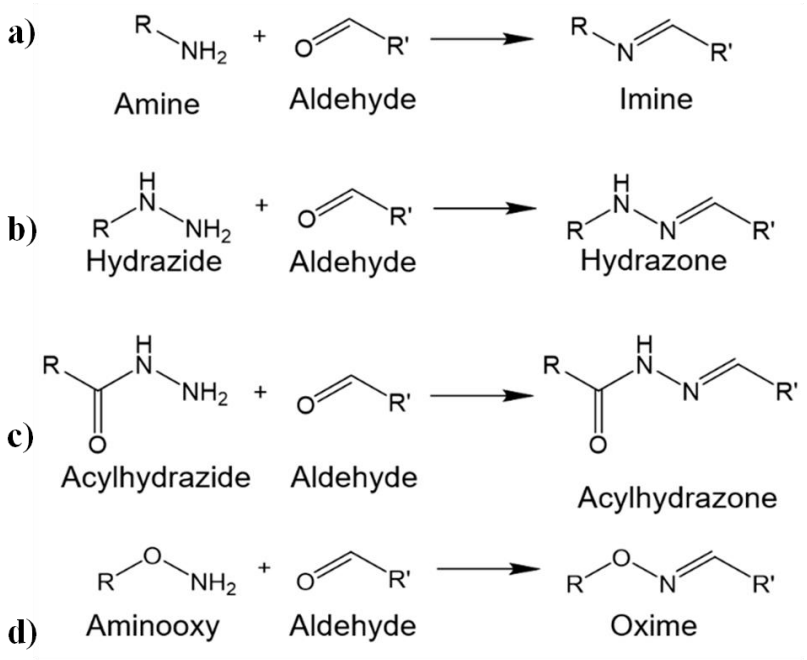

Fig.1.11: Formation of imine, hydrazone, acylhydrazone and oxime bonds from the reaction of an aldehyde with a primary amine, hydrazide, acylhydrazide and aminooxy group, respectively.

The dynamic nature of the C=N double bond also gives the characteristic property of self-healing to the hydrogels [67]. In addition, the Schiff base is pH-responsive, with oximes and hydrazones being more chemical stable at pH changes, compared to imines [68]. These are just some of the attributes that make Schiff base hydrogels excellent candidates for use in the biomedical field, such as drug delivery and tissue engineering [69], [70].

1.8. Aim of this study

As mentioned above, ocular drug delivery possesses several obstacles that hinder the efficient drug dosage. Different approaches have been developed to overcome these problems, including polymeric nanocarriers, implants and contact lenses. This work focuses on developing a polymeric delivery system for flurbiprofen and its sustained release into the eye.

The first part involves the encapsulation of flurbiprofen into nanosized, spherical nanocarriers based on biodegradable and FDA approved polyesters. More specifically, we implemented biocompatible and biodegradable polymers from PEG and PLLA in order to synthesize amphiphilic diblock and triblock copolymers via ring opening polymerization of L-lactide catalyzed by DMAP. The products were characterized by SEC and ^{1}H NMR spectroscopy. Next, the self-assembly of the copolymers was study by preparing polymeric micelles with the non-selective/selective solvent method. The morphology of the nanocarriers was studied by scanning electron microscopy (SEM) and transmission electron microscopy (TEM), while their size was determined by dynamic light scattering (DLS) measurements. The nanocarriers were then loaded with flurbiprofen and the release profile of the drug was monitored by fluorescence spectroscopy.

In the second part, aiming to develop a drug delivery system with a more prolonged drug release profile, hydrogels based on the natural polymer dextran were fabricated and were used as scaffolds for the encapsulation of either the drug or the drug-loaded PEG-*b*-PLLA micelles. To fabricate the hydrogels, first, the hydroxyl groups of dextran were modified using sodium periodate as the oxidation agent to produce aldehyde groups. Then, hydrogels were prepared by reacting ald-Dextran with adipic acid dihydrazide (AAD) under physiological conditions leading to the formation of acylhydrazone linkages. The successful formation of the linkages was verified by FTIR spectroscopy and the hydrogel's morphology was studied with SEM. The release profile of the drug from both drug carriers was monitored by fluorescence microscopy.

Chapter 2: Experimental Part

2.1. Materials

Poly(ethylene glycol) methyl ether (MePEG) with molecular weight of 5000 gr/mol was purchased from Polysciences Inc. PEG with molecular weight 4000 gr/mol was purchased from Sigma-Aldrich. L-lactide and DMAP catalyst were obtained from Sigma-Aldrich. AAD and sodium meta-periodate was purchased from Sigma-Aldrich, while dextran with molecular weight 40000 gr/mol was purchased from Serva. Flurbiprofen was gifted from the School of Medicine, University of Crete. Tetrahydrofuran (THF) (HPLC grade ≥ 99.9%) and petroleum ether were purchased from Scharlau S. L. THF (analytical grade) was purchased from Carlo Erba Reagents and deuterated chloroform (≥ 99.8%) was obtained from Deutero GmbH. Finally, dichloromethane (≥ 99.9%) was purchased from Sigma-Aldrich. Milli-Q water with a resistivity of 18.2 MΩ.cm at 298 K was obtained from a Millipore apparatus and was used for all experiments.

2.2. Synthesis of poly(ethylene-glycol) methyl ether-*b*-poly(L-lactide) (MePEG-*b*-PLLA) diblock copolymers and PLLA-*b*-PEG-*b*-PLLA triblock copolymers

MePEG was used as the macroinitiator and DMAP as the catalyst in a ring-opening polymerization of L-lactide to produce the MePEG-*b*-PLLA diblock copolymers. Briefly, the reaction vessel was filled with freeze-dried MePEG (0.33 gr, 7.6 mmol), recrystallized L-lactide (1 gr, 13.9 mmol), and catalyst (1%). Following a 30-minute N_2 purge, the reaction was then heated to 130 °C for 24 h, while being stirred in an oil bath. The final product was then precipitated in petroleum ether after being dissolved in dichloromethane. The product was placed under vacuum to dry, while the supernatant was discarded.

The synthesis of the PLLA-*b*-PEG-*b*-PLLA triblock copolymer was carried out using the same method, except that bifunctional PEG rather than monofunctional MePEG was used as the macroinitiator. More specifically, the vessel was filled with freeze-

dried PEG (0.4 g, 9 mmol), recrystallized L-lactide (1 g, 13.9 mmol), and catalyst (1%), and was then purged with N_2 for 30 min and heated in an oil bath at 130 °C for 24 h, while being stirred. The final product was dissolved in dichloromethane and precipitated in petroleum ether. The precipitated polymers were characterized by SEC and ^{1}H NMR spectroscopy.

2.3. Preparation of the PEG-*b*-PLLA and PLLA-*b*-PEG-*b*-PLLA nanocarriers

The non-selective-selective solvent dissolution method was used to synthesize the nanocarriers. In a nutshell, 2.5 ml of THF was used to dissolve 20 mg of the polymer, either diblock or triblock copolymer. Then, 15 ml of milli-Q water (pH 7.4) were supplied at a rate of 0.05 ml/min, using a syringe pump. The organic solvent was then evaporated using a rotary evaporator. After filtering through a hydrophilic Chromapure PVDF/L filter with 0.45 m pore size, the solution was placed in the refrigerator and was stored until use. The same method was used to prepare mixed nanocarriers made of both the triblock PLLA-*b*-PEG-*b*-PLLA and the diblock MePEG-b-PLLA copolymers by mixing equal amounts of the polymers. DLS was used to determine the nanocarriers' size, SEM and TEM were each used to confirm the nanocarriers' structure and morphology.

2.4. Preparation of flurbiprofen loaded PEG-*b*-PLLA and PLLA-*b*-PEG-*b*-PLLA nanocarriers

A stock solution of the drug at a concentration 1 mg/ml was prepared in THF. The non-selective-selective solvent dissolution approach was used to encapsulate the flurbiprofen drug. In brief, 20 mg of the polymer - diblock or triblock copolymer - were dissolved in 2.5 ml of THF, and 400 µl of stock solution were added to the polymer solution, followed by the same technique as stated above for the polymeric micelles. Additionally, flurbiprofen-loaded micelles made from both copolymers were prepared by dissolving 10 mg of each polymer in 2.5 ml of THF and adding 400 µl of the flurbiprofen stock solution. The same procedure was followed as described before to obtain the drug nanocarriers.

The %drug loading of the nanocarriers was determined using the following equation:

$$Drug\ loading = \frac{Weight\ of\ the\ drug\ in\ the\ nanocarriers}{Weight\ of\ the\ nanocarriers} * 100\%$$

2.5 Oxidation of Dextran

The oxidation of dextran by periodate was used to modify the polysaccharide to bear aldehyde groups. We aimed at an oxidation degree of 50%. To achieve this, 4 gr of dextran with a molecular weight of 40000 gr/mol were dissolved in 400 ml of ultrapure water at pH 5.5. Then, 4.74 gr of sodium meta-periodate was added to the reaction flask and it was left under stirring overnight. The final solution was placed in a dialysis bag and was dialyzed against milliQ water for 5 days. Finally, the product was freeze-dried and stored under ambient conditions.

2.6 Determination of the degree of oxidation

To determine the degree of oxidation of dextran, we employed the following titration protocol [71]. First, 0.125 gr of oxidized dextran was dissolved in 10 ml NaOH solution 0.25 M. Next, 15 ml HCl (0.25 M) and 50 ml of milliQ water was added. Finally, 1 ml of a 0.2% phenolphthalein solution in NaOH was added into the vessel to observe the color change. The solution was titrated against a 0.25 M NaOH solution until a color change was observed from yellow to dark pink/purple. The same procedure was followed using original dextran.

The degree of oxidation was calculated using the following equation:

$$OD = \left[\frac{(N_b - N_a)_s}{W_s/_M} - \frac{(N_b - N_a)_p}{W_p/_M}\right] \times 100\%\ ,$$

were N_b is the total amount of NaOH (mol), N_a is the total amount of HCl (mol), W is the dry mass of the polymer (mg) and M is the molecular weight of the sugar unit (162 gr/ml). The symbol *s* denotes oxidized dextran, while *p* denotes dextran before oxidation.

2.7 Synthesis of dextran-based hydrogels

For the synthesis of the hydrogels, we prepared aqueous solutions of Ald-Dex (91 mg/ml) and AAD (100 mg/ml). Next, a predetermined amount of the AAD solution was added to the Ald-Dex solution in order to form hydrogels with different degree of cross-linking (10, 20 and 30 wt %). The gels were allowed to sit for 1 h and the successful gelation was confirmed by the inverted tube method. Finally, the hydrogels were washed with water (10 times) to remove the non-crosslinked polymer and freeze-dried. The hydrogel's structure and morphology were characterized by FTIR and SEM, respectively.

2.8 Preparation of Flurbiprofen loaded hydrogels

We utilized two different approaches to incorporate drug molecules within the hydrogel. The first method included the use of Flurbiprofen loaded PEG-*b*-PLLA micelles. A concentrated solution of the micelles was used as the medium to dissolve dextran. Next, AAD was added into the solution leading to the hydrogel formation. A similar method was implemented for the second approach. This time, the drug was directly dissolved in the polymer solution, followed by the addition of AAD and the formation of the hydrogel. The hydrogels were left to sit for 1 h and were placed in a vial with water to initiate the release experiment.

2.9 Release of Flurbiprofen

To study the release profile of the drug from the polymeric nanocarriers, 4 ml of the prepared micellar solutions were transferred into a dialysis membrane with MWCO of 3.500 gr/mol. Then, 40 ml of milli-Q water at pH 7.4 was added to the vial containing the dialysis membrane. The vial was then placed in a water bath which was kept at a constant temperature of 37 °C to mimic the body temperature. The water medium was removed from the vial and fresh water was added at predetermined time intervals. The collected samples were evaporated under vacuum. Using a calibration curve for flurbiprofen in THF, the dried samples were dissolved in 3 ml THF and the amount of released flurbiprofen was measured by fluorescence spectroscopy.

To study the release of the drug from the hydrogels, the gels were placed in a vial and 5 ml of water at pH 7.4 was added. The vial was then placed in a water bath at a constant temperature of 37 °C. At certain time intervals, the water medium was withdrawn from the vial and was replaced with fresh water. The dried samples were dissolved in 3 ml THF, and the amount of flurbiprofen released was determined using fluorescence spectroscopy. The amount of drug released was calculated based on the calibration curve in THF seen in **Fig. 2.1**. The % released drug was determined from the equation:

$$Released\ flurbiprofen\ (\%) = \frac{Released\ amount\ at\ specific\ time}{Total\ amount\ of\ loaded\ drug} * 100\%$$

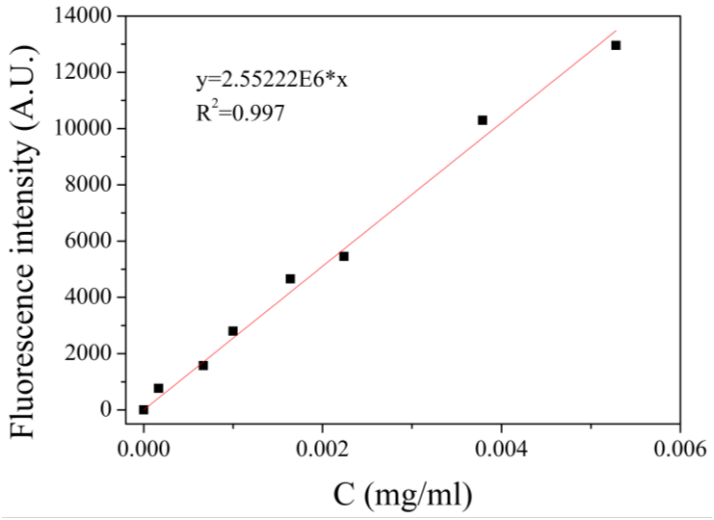

Fig. 2.1: Calibration curve of flurbiprofen in THF

2.10 Characterization methods

2.10.1 Size Exclusion Chromatography (SEC)

In order to determine the molecular weights and the PDIs of the polymers, SEC, equipped with a Waters 515 isocratic pump, two columns, Mixed-D and Mixed-E (Polymer Labs), a Waters 2745 Dual Absorbance detector and a Waters 410 refractive index (RI) detector, was used. THF (HPLC grade) with 2% v/v TEA was used as the eluent at a flow rate of 1 ml/min and the column temperature was set at 25 °C. Typically 20 mg of the polymer were dissolved in 1 ml THF (HPLC). Next, the solution was filtered through a 0.45 μm pore size PTFE filter and was consequently injected into the system. The molecular weights of the polymers were calculated using a calibration curve based on PMMA standards with molecular weights ranging from 625 to 138600 gr/mol.

2.10.2 Proton Nuclear Magnetic Resonance (^{1}H NMR) spectroscopy

The polymers were characterized by ^{1}H NMR spectroscopy on an Avance Bruker 300 MHz spectrometer using tetramethylsilane (TMS) as an internal standard and $CDCl_3$ as the solvent.

2.10.3 Field emission scanning electron microscopy (SEM)

SEM images were obtained using a JEOLJSM-7000F microscope. A drop of the micellar sample was deposited on a glass slide and was left to dry overnight at room temperature. Then the sample was sputter-coated with Au (10 mm thick) before imaging. For the hydrogel samples, a small piece of the hydrogel was deposited on a glass slide and was sputter-coated with Au (30 mm thick).

2.10.4 Dynamic Light Scattering (DLS)

The size of the micelles was measured using a Malvern Zetasizer Nano ZS instrument equipped with a 4 MW He-Ne laser operating at λ = 632.8 nm. The scattering angle was 90° and three scans were collected for each measurement.

2.10.5 Transmission Electron Microscopy (TEM)

TEM images were captured with a JEOL JEM-2100 instrument at 80 KV. A drop of the sample was deposited on a carbon-coated cooper grid and was left to dry overnight.

2.10.6 Fourier Transform Infrared Spectroscopy (FTIR)

The synthesis of the Ald-Dex hydrogels was confirmed by FTIR spectroscopy. FTIR spectra were recorded on a Thermo and Scientific Nicolet 6700 FTIR spectrometer. The scanning range was 4000-400 cm^{-1} at a resolution of 4 cm^{-1}. A total of 64 scans were collected.

2.10.7 Fluorescence spectroscopy

The fluorescence spectra were recorded using a Lumina Fluorescence Spectrometer by Thermo Fisher Scientific. The excitation and emission wavelengths were set at 248 and 260 nm, respectively. The emission and excitation slits were both set to 5 nm and 20 nm. The response time was set at 2 s. The samples were measured in quartz cuvettes.

Chapter 3: Results and Discussion

3.1 Synthesis and characterization of MePEG-*b*-PLLA diblock and PLLA-*b*-PEG-*b*-PLLA triblock copolymers

As mentioned above, ring-opening polymerization was used to synthesize MePEG-*b*-PLLA diblock and PLLA-*b*-PEG-*b*-PLLA triblock copolymers. The synthesis of the MePEG-*b*-PLLA diblock copolymer is shown schematically in **Fig. 3.1a**, whereas the synthesis of the triblock copolymers is shown schematically in **Fig. 3.1b.** PEG was used as the initiator for the polymerization of the L-lactide monomer. The polymerization of the diblock copolymer is initiated by the hydroxyl group of MePEG. A bifunctional PEG was used in the case of the triblock. The hydroxyl groups PEG on both ends initiated the L-lactide polymerization on both sides of the polymer.

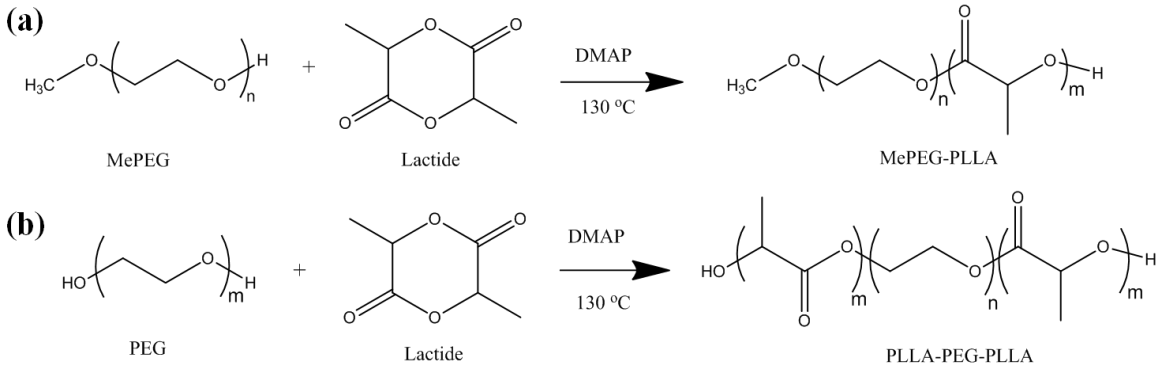

Fig. 3.1: Synthesis of the (a) MePEG-*b*-PLLA diblock copolymer and (b) PLLA-*b*-PEG-*b*-PLLA triblock copolymer.

The successful synthesis of the copolymers was confirmed by SEC. The molecular weight of the MePEG-*b*-PLLA diblock copolymer was found 26,500 g/mol with a PDI 1.41. On the other hand, the molecular weight of the PLLA-*b*-PEG- *b*-PLLA triblock copolymer was found 14,000 g/mol with a PDI of 1.33. The chromatogram of the diblock copolymer is shown in **Fig. 3.2a,** whereas the chromatogram of the PLLA-*b*-PEG-*b*-PLLA triblock copolymer is shown in **Fig. 3.2b**. As observed by SEC the peak of MePEG appeared at elution time 14.1 min, while the copolymer peak

appeared at 13.3 min. The shift of the copolymer peak at lower elution times, and thus higher molecular weights, confirms the successful polymerization of the lactide monomer from the PEG macroinitiator. Similarly, for the triblock copolymer, the SEC peak of the PEG block appeared at elution time 15 min, while the copolymer peak appeared at lower elution time, 13.3 min, again verifying the successful chain growth.

The SEC curves of the block copolymers and the PEG macroinitiators slightly overlap, indicating the presence of unreacted PEG and a small amount of PLLA homopolymer. As already discussed above, ROP is initiated from the hydroxyl groups, thus traces of water molecules in the reaction could also initiate the polymerization, resulting in the production of PLLA homopolymers. To purify the copolymers further, the precipitation process was performed in threefold.

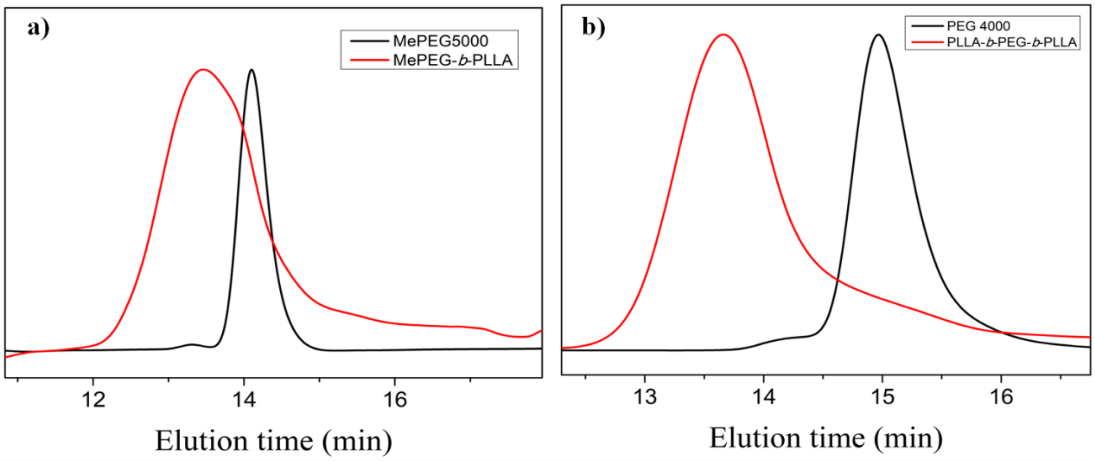

Fig. 3.3: SEC curves of a) the MePEG-*b*-PLLA diblock and b) the PLLA-*b*-PEG-*b*-PLLA triblock copolymer, together with the respective PEG macroinitiators

The chemical structure and the composition of the diblock and triblock copolymers were determined by ^{1}H NMR spectroscopy. **Fig. 3.3a** shows the ^{1}H NMR spectrum of the diblock copolymer. The peak at 1.6 ppm (a) is assigned to the methyl protons of the L-lactide monomer repeat unit, the peak at 5.18 ppm (b) refers to the proton of the –CH group of the lactide units, while the peak at 3.66 ppm (c) is assigned to the CH_2 protons of the PEG block. Similar, for the triblock copolymer, the peak of the methyl group of the L-lactide monomer repeat units at 1.58 ppm (a), the peak of the proton of the –CH group of the lactide units at 5.19 ppm (b), and the four protons of PEG at 3.66 ppm (c), are observed (**Fig. 3.3b**).

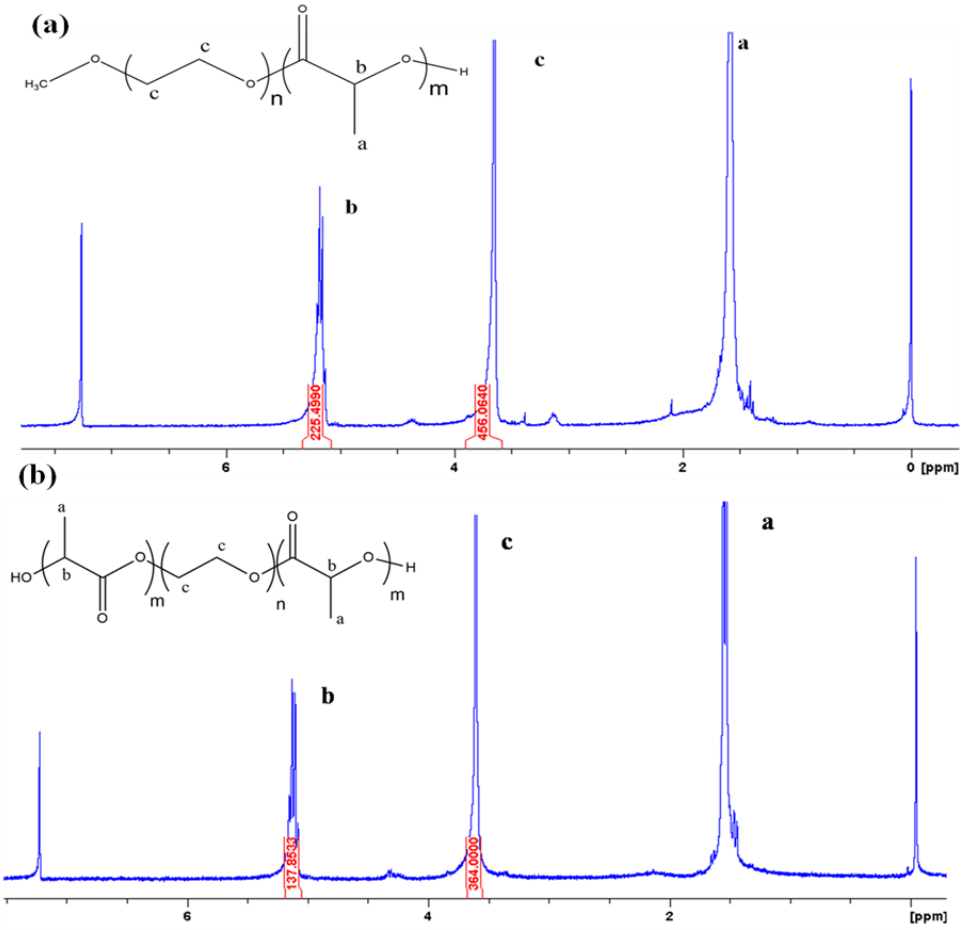

Fig. 3.3: ^{1}H NMR spectra of a) Me PEG-*b*-PLLA diblock and b) PLLA-*b*-PEG-*b*-PLLA triblock copolymer

We can calculate the number of protons assigned to PLLA and hence determine the molecular weight of the diblock and triblock copolymers by determining the number of hydrogen atoms in the product that are assigned to PEG and rationing the integrals of the appropriate peaks. **Table 3.1** summarizes the molecular weights, the degree of polymerization, polydispersity index (PDI) as well as the % monomer conversion for all synthesized copolymers.

Table 3.1. Molecular characteristics of the diblock and triblock copolymers.

Polymer	**DP_{PEG}**	**DP_{PLLA}**	**M_n (by SEC) (gr/mol)**	**M_w/M_n (by SEC)**	**% Conv (by ^{1}H NMR)**
Diblock	114	208	26,500	1.38	97%
Triblock	91	138	14,000	1.57	99%

3.2 Self-assembly of the MePEG-*b*-PLLA diblock and PLLA-*b*-PEG-*b*-PLLA triblock copolymers.

The ability of the amphiphilic copolymers to self-assemble into nanosized structures was studied. The nanocarriers were prepared using the non-selective-selective solvent method. This process yields micelles that are uniform in size and possess a low PDI. The average size of the micelles formed by the diblock copolymer was found 160 nm, as illustrated in **Fig. 3.4a**. This size is quite large compared to the size of the copolymer chains and was thus attributed to the formation of micellar aggregates in the aqueous solution. The spherical shape of the micelles was confirmed by SEM and TEM also shown in **Figs. 3.4b** and **3.4c**.

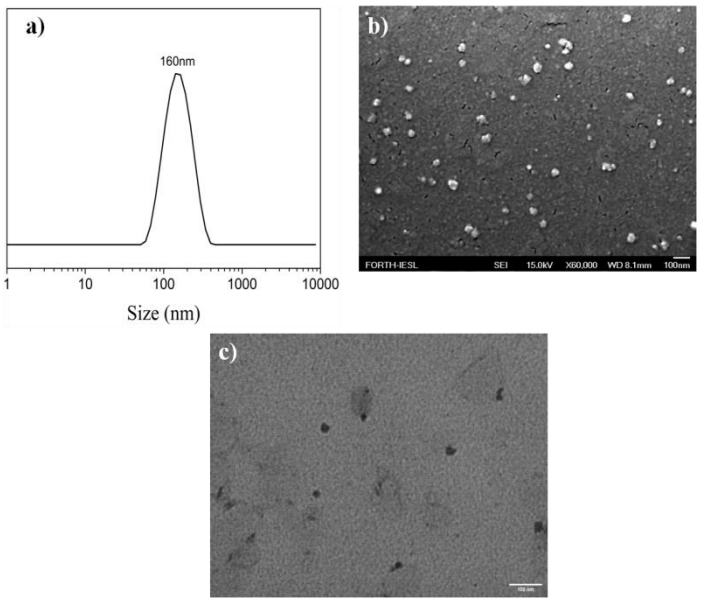

Fig. 3.4: a) DLS measurement b) SEM image and c) TEM image of the MePEG-*b*-PLLA diblock copolymer micelles, (scale bars: 100 nm).

The triblock copolymer also formed nanostructures as shown in **Fig. 3.5b**. In this case, there were two size distributions observed in DLS (**Fig. 3.5a**), one at 25 nm and one at 191 nm. The smaller size was assigned to the polymer micelles, whereas, the larger size was attributed to the formation of micellar aggregates within the aqueous medium.

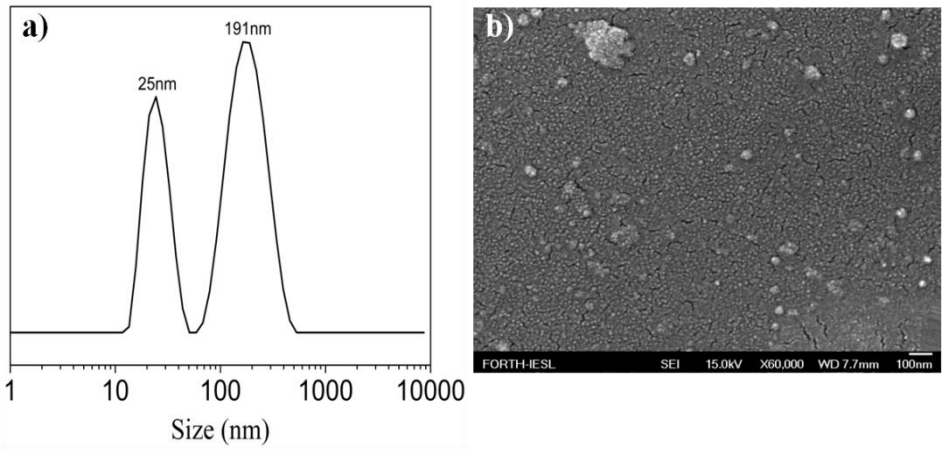

Fig. 3.5: a) DLS measurment and b) FE-SEM image of the PLLA-*b*-PEG-*b*-PLLA triblock copolymer micelles (scale bar: 100 nm).

Furthermore, the self-assembly behavior of a mixture of the diblock and triblock copolymers in water was examined in order to form more complicated nanocarrier structures. The obtained nanostructures were again spherical in shape forming micellar nanoparticles as observed by SEM (**Fig. 3.6b)**. Their average size was 170 nm, which is between that of the size of the diblock and the triblock copolymer nanoparticles.

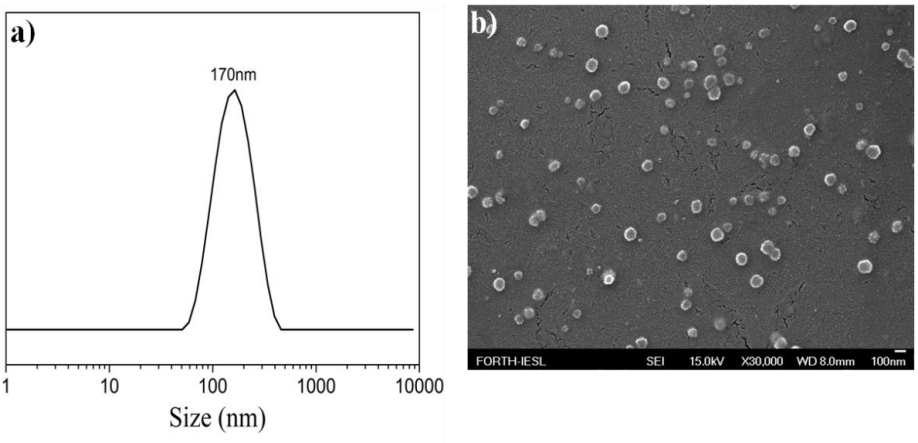

Fig. 3.6: a) DLS measurement and b) FE-SEM image of mixed diblock and triblock copolymer nanoparticles (scale bar: 100 nm).

3.3 Release study of flurbiprofen from the polymeric micelles

The above results demonstrated the effective self-assembly of the diblock, triblock, as well as the mixed diblock and triblock copolymers, and the formation of spherical nanostructures. The drug release profiles from the three formulations was then investigated. **Fig. 3.7** shows the flurbiprofen release kinetics from the polymeric nanocarriers. First, the encapsulation and the release profile of flurbiprofen from the diblock copolymer nanoparticles was examined. The drug loading was found 0.21% (42 μg of drug). As observed in **Fig. 3.7**, 90% of the drug was released during the first 24 h. This result was attributed to the passive diffusion of flurbiprofen from the polymeric micelles into the aqueous media. As shown, the release profile attained a plateau in about four days. Next, the release profile of flurbiprofen from the triblock copolymer nanoparticles was examined. The drug loading of the triblock copolymer micelles was found 0.14%, which corresponds to 27 μg of the drug. As observed in **Fig. 3.7**, the rate of the released drug from the triblock copolymer micelles was similar to that found for the diblock copolymer nanoparticles. The lower drug loading in the triblock copolymer nanocarriers, can be attributed to the fact that the PLLA block had a lower molecular weight compared to the diblock copolymer, which resulted in the formation of smaller hydrophobic core, therefore poorer encapsulation effectiveness. However, it is important to note that both polymeric nanoparticles delivered fully the medication in 4 days, despite their different drug loadings.

From the above results, we can conclude that the diblock and triblock copolymer nanocarriers are not able to encapsulate a significant amount of flurbiprofen neither to sustain the drug release rate. To overcome this limitation, we hypothesized, that perhaps a more complex nanoparticle structure, could prolong the release profile of the drug. Thus, we prepared mixed nanoparticles comprising of the diblock and triblock copolymer chains (**Fig. 3.7)**. However, we found that this self-assembled system exhibited a much lower drug loading of 0.05% (10 μg of drug), while it also released approximately 90% of its payload in the first 24 h. It is assumed that the complexity of the nanocarriers structure did not allow to encapsulate a large amount of drug inside the hydrophobic core during the self-assembly process, which also led to a fast release kinetics. However, additional investigation is required to ascertain the

drug encapsulation and release behavior from such mixed nanoparticles and to further understand the mechanism underlying it.

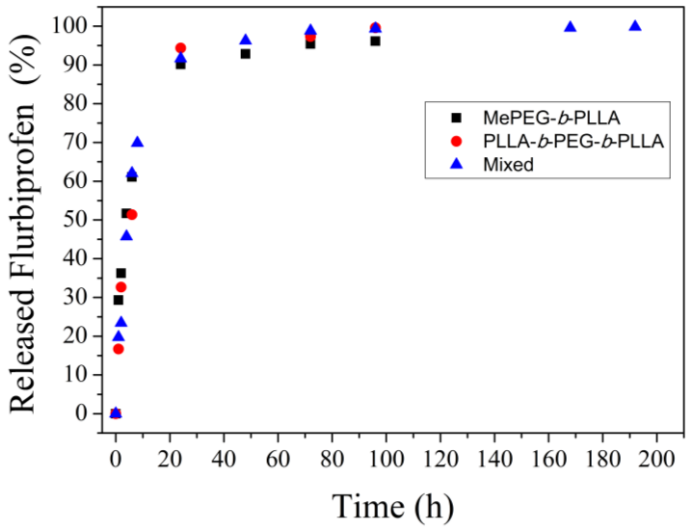

Fig. 3.7: Release profile of flurbiprofen from the polymeric nanoparticles formed by the MePEG-*b*-PLLA diblock copolymer, the PLLA-*b*-PEG-*b*-PLLA triblock copolymer and the mixed diblock and triblock copolymer system.

3.4 Synthesis and characterization of dextran hydrogels

In the previous part of this thesis, it was found that none of the polymeric nanocarriers formed was capable to slow down the release profile of the drug above 24 h. To overcome this challenge, we aimed to prepare hydrogels comprising the natural polysaccharide dextran, and to incorporate the drug-loaded polymeric micelles within the hydrogel in order to prolong the drug release profile. First, dextran was oxidized using sodium periodate, which resulted in the formation of aldehyde groups along the backbone of the polymer chain and the formation of oxidized dextran (Ald-Dex). The degree of oxidation was found by the titration method to be 53%. The successful oxidation of dextran was confirmed by FTIR spectroscopy (**Fig. 3.8**). The vibration peak observed at 3380 cm^{-1} corresponds to the hydroxyl groups of the polymer. When comparing that to the pure dextran sample, the peak of the modified polymer is found much broader. This is due to the overlap of the peak of the absorbed water molecules by the material to that of the hydroxyl polymer groups. The appearance of a new peak at 1716 cm^{-1} is also observed in **Fig. 3.8**, which is assigned to the stretching vibration of the C=O aldehyde group, and verifies the successful

modification of dextran. The vibrations at 2920 and 1020 cm^{-1} correspond to the C-H and C-O-C stretching vibrations of the pyranose ring, respectively [72].

Following the modification of the polymer, we proceeded with the preparation of the Ald-Dex hydrogels using AAD as the crosslinking agent. We prepared hydrogels using 10-30 wt% cross-linker with respect to the modified natural polymer. The successful synthesis of the hydrogel was confirmed by FTIR spectroscopy. The spectra of dextran, Ald-Dex and the 30 wt% crosslinked hydrogel are shown in **Fig. 3.8**. The aldehyde groups of the polysaccharide reacted with the hydrazide groups of AAD to form acylhydrazone bonds, which have a characteristic peak at 1600-1650 cm^{-1}. The peak at 1646 cm^{-1} observed in **Fig. 3.8** is assigned to the formation of the acylhydrazone bonds.

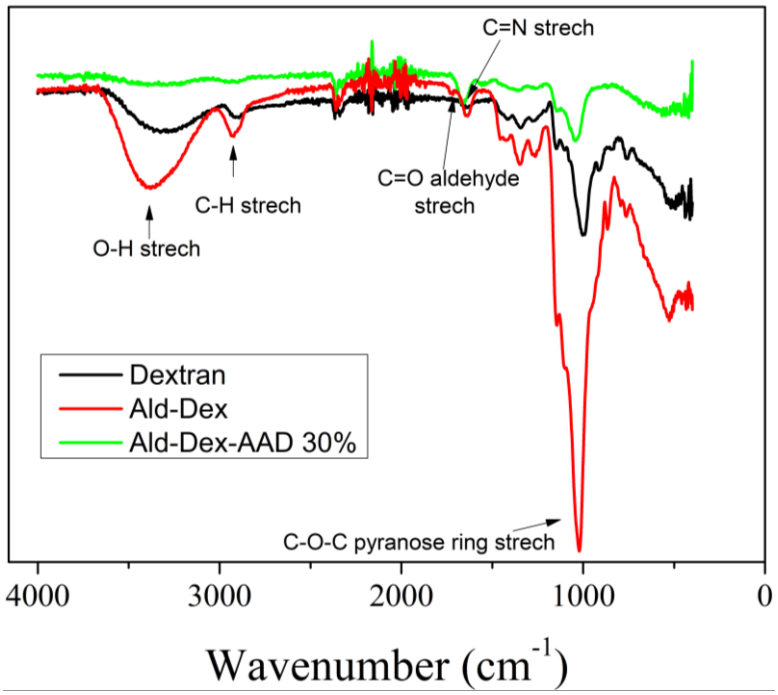

Fig. 3.8: FTIR spectra of Dextran, Ald-Dex and the Ald-Dex-AAD hydrogel.

Next, the morphology of the hydrogels was studied by SEM (**Fig. 3.9**). As seen in **Fig. 3.9a**, the hydrogel with 10 wt% cross-linker presented a larger pore size distribution, ranging from 2-11 μm and more well-defined pores compared to the 20 wt% cross-linker ratio, which gave a pore size of about 0.4 μm (**Fig. 3.9b)** and the 30 wt% cross-linker with pore size 1.5-3 μm (**Fig. 3.9c)**.

As expected, it was found that when increasing the amount of cross-linker from 10 wt% to 20 wt%, denser and with smaller and less pores hydrogels, were obtained. However, the 30 wt% hydrogel had larger pores and a higher pore size polydispersity (**Fig. 3.9d)** compared to the 20 wt% hydrogel. This indicates that a potential excess of the crosslinker molecules led to a decreased cross-linking efficiency, thus resulting in a less dense hydrogel. This resulted in a hydrogel with a higher porosity [73].

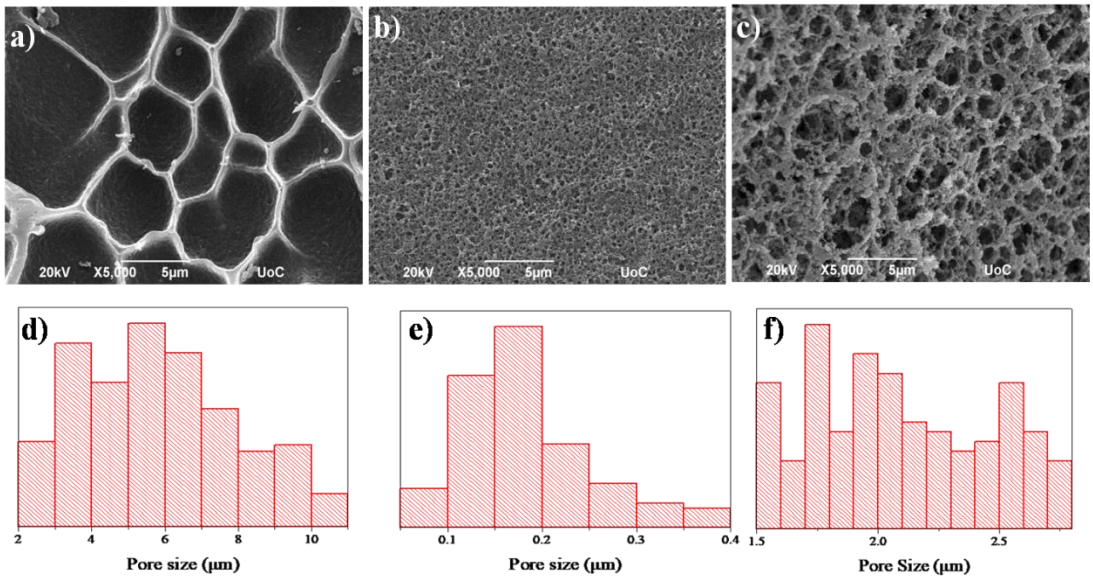

Fig. 3.9: SEM images of the Ald-Dex-AAD hydrogels with a) 10 wt% cross-linker, b) 20 wt% cross-linker and c) 30 wt% cross-linker. Size distribution histograms of the pore size for the Ald-Dex-AAD hydrogels with 10 wt% cross-linker, b) 20 wt% cross-linker and c) 30 wt% cross-linker, obtained by SEM.

3.5 Release study of flurbiprofen from the Ald-Dex-AAD hydrogels

To investigate the release profile of flurbiprofen from the hydrogels, we prepared dextran-based hydrogels loaded with the drug, following two different approaches. In the first method we focused on the encapsulation of the drug molecules within the hydrogel matrix during the formation of the hydrogel. The second method, involved the incorporation of the drug loaded MePEG-*b*-PLLA micelles within the hydrogel pores. We sought to delay the release of flurbiprofen from the polymeric materials, therefore, in the first approach we examined the release profile of the drug from the 20 wt% and the 30 wt% hydrogels, while for the second method we focused on the 30 wt% hydrogel. The results from this first set of experiments, in which the drug was

loaded within the polymer hydrogel directly, are shown in **Fig. 3.10**. As it can be seen, these systems were not able to slow down the release of the drug molecules, and the cargo was released quantitatively in just under 4 h. It is worth noting, that the amount of cross-linker had a very small impact on the performance of these hydrogels and did not affect the cumulative release of the drug, neither its release profile.

In the case of the hydrogel loaded with the polymeric nanoparticles, when comparing the release profile with that of the polymeric nanoparticles alone, we observed that the hydrogel exhibited a similar burst release during the first few hours of the experiment, owing to the passive diffusion of the drug molecules, however, the hydrogel achieved to slow down the release profile of flurbiprofen (**Fig. 3.10**). About 60 % of the drug was released from the nanoparticle loaded hydrogel within 24 h, while the polymeric nanoparticles alone showed an almost 90 % drug release at the same time. Overall, the nanoparticle loaded hydrogel achieved a total of 95 % release of the drug in 7 days. Therefore, we can conclude, that in comparison with the drug loaded hydrogel as well as the drug loaded nanocarriers alone, the combination of the drug loaded nanocarriers and a highly cross-linked hydrogel greatly improved the sustained release of the drug.

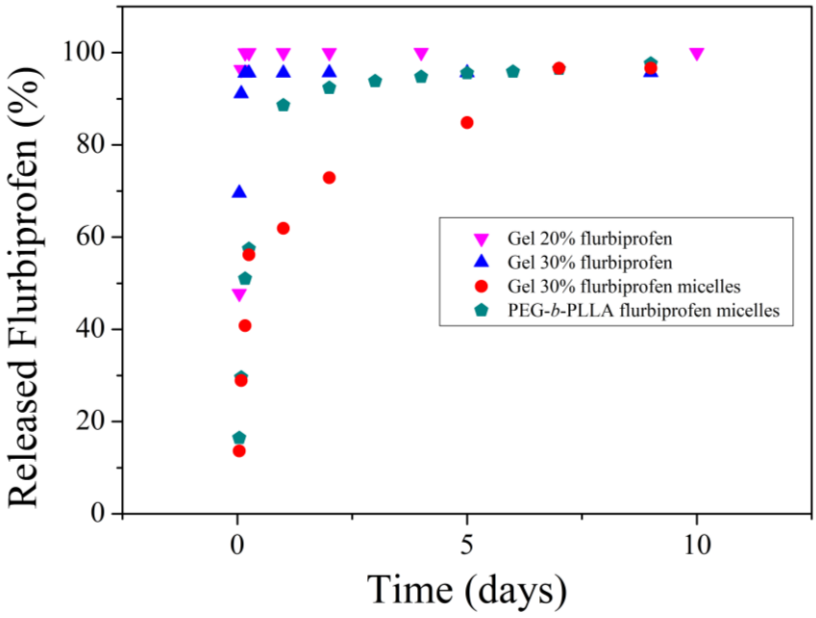

Fig. 3.10: Flurbiprofen release profile from the nanoparticle loaded hydrogel in comparison with the flurbiprofen loaded PEG-*b*-PLLA nanoparticles and the drug loaded hydrogels alone

Chapter 4: Conclusions and Future Perspectives

The delivery of drugs to the eye has proven to be a challenging issue for scientists due to the eye's complex structure. Liposomes, polymeric nanoparticles, polymeric micelles and vesicles are among the most widely used nanocarriers for the effective transportation of pharmaceutical substances into the ocular area. Polymeric micelles comprising biodegradable, amphiphilic block copolymers have been extensively used as medicinal carriers. The main purpose of this thesis was to develop a drug delivery system based on biodegradable diblock and triblock copolymers for the sustained release of flurbiprofen into the eye.

Copolymers of MePEG-*b*-PLLA and PLLA-*b*-PEG-*b*-PLLA were synthesized and characterized using SEC and ^{1}H NMR spectroscopy. To accomplish the block copolymer self-assembly in water, the non-selective-selective solvent dissolution approach was employed. The size of the nanocarriers was determined using DLS, and their morphology was confirmed by SEM and TEM. The diblock copolymer produced nanoparticles with a diameter of 160 nm, while the triblock copolymer formed nanoparticles with diameters of 25 nm and 190 nm. Finally, the two copolymers were combined to form mixed nanoparticles with a diameter of 170 nm.

To investigate the kinetics of flurbiprofen release from the polymeric nanocarriers, the diblock, triblock and mixed nanoparticles were loaded with the drug and were immersed in a water bath at 37 °C to mimic the body temperature. The findings showed that all three polymeric systems gave a 100% release of their payload within 4 days, despite their different drug loading capacity.

Next, to further delay the release of the drug, we employed hydrogels comprising the natural polymer dextran which was cross-linked using adipic acid dihydrazide (AAD). The polymer was first oxidized with sodium periodate to generate aldehyde groups along the polymer chains. These groups were used to cross link the polymer by reaction with the hydrazide groups of AAD resulting in the formation of acylhydrazone bonds. The hydrogels were characterized by SEM and FTIR spectroscopy. By varying the amount of AAD with respect to the polymer, we prepared hydrogels of 10-30% wt% cross linker content. The drug release study involved the incorporation of flurbiprofen loaded nanoparticles within the hydrogel as

well as the direct loading of the drug in the hydrogel matrix. The hydrogel-drug system was not able to slow down the release profile of the drug molecules, owing to the simple diffusion of the drug through the pores of the hydrogel to the external aqueous medium. In comparison, the nanoparticle loaded hydrogel system was able to further delay the release profile of flurbiprofen and reached a 95% drug release in 7 days, showing some promising results for the use of this system as a drug delivery platform in ocular treatment.

Future work will focus on the optimization of the drug loading within the polymeric nanoparticles. In addition, further research is required to better characterize the dextran-based hydrogels, including swelling and rheological experiments as well as their stability and degradation profiles in the aqueous media.

APPENDIX: Characterization Techniques

1) Size Exclusion Chromatography (SEC)

Size exclusion chromatography (SEC), or gel permeation chromatography (GPC), is a well-known polymer separation method that allows determination of the polymer molecular characteristics, such as the average molecular weight and molecular weight distribution. In general, SEC is an important analytical tool used to evaluate the molecular characteristics of natural or synthetic polymers and proteins. A SEC instrument comprises a pump, a detector (e.g., UV or RI or both) and one, two or more separating columns. The columns or the stationary phase are filled with porous beads such as polystyrene particles. The beads are made with a variety of pore sizes that span the range of the sizes of the macromolecules to be separated. The pump circulates solvent (mobile phase) through the columns and swells the material in the column. A small amount of diluted polymer solution in the same solvent as the mobile phase is injected in the flowing solvent entering the columns. As the polymer solution passes through the columns, the largest polymer particles are excluded from all, but the largest pores and elute from the column first. Right after, smaller polymer coils can pass through smaller pores and are excluded later from the columns. In this way, SEC separates the molecules by their size in solution, which is their hydrodynamic volume (V_h). After separation, the solution passes through the detectors used in the system and are analyzed, upon proper calibration with narrow molar mass distribution standards.

2) ^{1}H NMR spectroscopy

NMR spectroscopy is a very useful technique commonly employed for the determination of the chemical structure of chemical compounds. NMR is a spectroscopic technique allowing to observe local magnetic fields around atomic nuclei. The sample with the material is placed in a magnetic field and the NMR signal is produced by excitation of the nuclei of the sample with radio waves into nuclear magnetic resonance, which is detected with sensitive radio receivers. The signal

provides the required information regarding the environment of the nuclei. The exact field strength (in ppm) of a nucleus comes into resonance relative to a reference standard, usually the signal of the deuterated solvent used. Electron clouds shield the nuclei from the external magnetic field causing them to absorb at higher energy (lower ppm), while the neighboring functional groups "deshield" the nuclei causing them to absorb at lower energy (higher ppm). Chemically and magnetically equivalent nuclei resonate at the same energy and give a single signal or pattern. ^{1}H NMR and ^{13}C NMR are most commonly used for the characterization of materials. Protons on adjacent carbons interact and split each other's resonances into multiple peaks following the n+1 rule with coupling constant J. Spin-spin coupling is commonly observed between nuclei that are one, two and three bonds apart. The area under an NMR peak is proportional to the number of nuclei that give rise to that resonance, thus by integration, the protons of that resonance can be calculated.

3) Dynamic Light Scattering (DLS)

Light scattering is a powerful tool for the characterization of the size of polymer nanoparticles in solution. The monochromatic, coherent laser beam hits the particles, and is scattered, due to the Brownian motion of the particles that changes their distance in the solution, and a time-dependent fluctuation of the scattering intensity is observed. By changing the observation angle (θ) and thus the scattering vector (q) a measure of the particle size is provided. The form factor, that is the interference pattern of the scattered light, is characteristic of the size and shape of the scatterers. The larger the particles are, the slower their Brownian motion. Accuracy and stability of the temperature during the entire measurement is essential since the viscosity of the liquid is related to the temperature. The velocity of the Brownian motion is defined by the translational diffusion coefficient (D). The Stocks-Einstein equation is used to calculate the particles' size based on the translational diffusion coefficient:

$$R_h = \frac{K_B T}{6\eta\pi D}$$

where, (R_h) is the hydrodynamic radius, (η) is the viscosity of the solvent, (K_B) is the Boltzmann constant and (T) is the temperature.

4) Field Emission Scanning Electron Microscopy (SEM)

Scanning electron microscopy is designed to provide high-resolution images of a sample placed on a surface. A tungsten filament emits electrons, which are focused by an electron optical system. The electron beam can scan the sample surface and can provide its composition at a point, along a line or over a rectangular area, by scanning the beam across the surface in a series of parallel lines. The sample is mounted on a stage that can be accurately moved in all three directions (x, y and z), normal to the plane of the sample. The instrument generally operates under high vacuum in a very dry environment in order to produce the high energy beam of electrons needed for imaging. However, most specimens destined for study by SEM are poor conductors. In SEM, the imaging system depends on the specimen being sufficiently electrically conductive to ensure that the bulk of the incoming electrons go to ground. The formation of the image depends on the collection of the different signals that are scattered as a consequence of the high electron beam interacting with the sample. The two principal signals used to form images are backscattered and secondary electrons generated within the primary beam-sample interactive volume. The backscattered electron coefficient increases with increasing the atomic number of the specimen, whereas the secondary electron coefficient is relatively insensitive to the atomic number. This fundamental difference in the two signals has an important effect on the way samples may need to be prepared. The use of scanning electron microscopy may be considered when being able to interpret the information obtained from the SEM, and attempt to relate the form and structure of the two-dimensional images and the identity, validity and location of the chemical data, back to the three-dimensional sample from which the information was derived. The biggest difference between a FESEM and a SEM lies in the electron generation system. As the source of electrons, FESEM uses a field emission gun that provides extremely focused, high- and low-energy electron beams, which greatly improves spatial resolution and enables work to be carried out at very low potentials (0.02–5 KV). This helps to minimize the charging effect on non-conductive specimens and to avoid damage from the electron beam on sensitive samples.

5) Transmission Electron Microscopy (TEM)

In TEM, the beam of electrons from the electron gun is focused into a small, thin, coherent beam by the use of the condenser lens. This beam is restricted by the condenser aperture, which excludes high angle electrons. The beam then strikes the specimen, and electrons are transmitted depending upon the thickness and electron transparency of the specimen. The transmitted portion is focused by the objective lens forming an image on a phosphor screen or a charge coupled device (CCD) camera. Optional objective apertures can be used to enhance the contrast by blocking out high-angle diffracted electrons. The darker areas of the image represent the areas of the sample where fewer electrons are transmitted, while the lighter areas of the image represent the areas of the sample where electrons were transmitted through.

6) Fluorescence spectroscopy

The technique of fluorescence spectroscopy is based on the phenomenon of fluorescence, i.e., the emission of radiation from an excited molecule. In general, when a molecule in the ground state of energy interacts with radiation of appropriate frequency, the molecule absorbs the radiated energy and is excited, that is, it transitions to a higher energy level. This excitation is maintained for a short time, as the molecule eliminates the absorbed energy either in the form of heat or through radiation emission and returns to the ground state. The de-excitation of the molecule through radiation emission is called photoluminescence and when it occurs in a short time (10^{-9}-10^{-6}s) from the moment of stimulation, it is characterized as fluorescence.
In more detail, the fluorescence phenomenon can be described as a three-step process. In the first stage, an energy photon supplied by an external radiation source is absorbed by the molecule in the ground state. The result of this absorption is the transition of an electron from the ground state to the first excited electron simple state. Each electronic state is separated into individual vibrational levels and the transition usually takes place to the highest energy vibrational level of the first excited state. In the second stage, during the life of the excited state, the molecule loses energy due to changes in its configuration or collisions with molecules in its environment. The loss of this energy leads to the transition of the electron from the highest to the lowest vibrational level of the first excited state and this process is called vibrational

relaxation. Finally, in the third stage, the de-excitation of the molecule takes place, i.e., the transition of the electron from the lowest energy vibrational state to the ground state, with parallel emission of energy radiation, which gives the fluorescence signal.

7) FTIR spectroscopy

Infrared refers to the region of the electromagnetic spectrum between visible and microwave. The IR region is divided into three regions: the near, mid, and far IR. The near IR covers the area of 14000-4000 cm^{-1}, the mid IR from 4000 to 400 cm^{-1} while the far-infrared lies between 400-10 cm^{-1}. Organic molecules absorb infrared radiation and turn it into energy of molecular vibration. An organic molecule is subjected to infrared light in IR spectroscopy. Absorption happens when the irradiation energy and the energy of a particular molecular vibration match.

An in-depth description of a molecule's vibrations can be obtained by infrared spectroscopy. Infrared spectroscopy can examine both the identification of the molecule and the molecule's structure due to the characteristic molecular vibrations that reflect chemical features, such as an arrangement of nuclei and chemical bonds inside the molecule. In order for a molecule's vibrations to be active in the infrared, a change in its electric dipole moment needs to take place. That is the reason why vibrations of only heteronuclear diatomic molecules appear in the infrared absorption spectra. Geometrically linear molecules with N atoms have 3N - 5 degrees of vibrational modes, whereas, nonlinear molecules have 3N - 6 degrees of vibrational modes. The vibrations can be either a) stretching or b) bending. Furthermore, the stretching vibrations can be categorized into symmetric and antisymmetric, while bending modes are classified as scissoring, rocking, wagging or twisting.

An FTIR spectrometer consists from the light source, usually silicon carbide, a Michelson interferometer, which consists of a beam splitter and one fixed and one movable mirror, and a detector that detects the transmitted radiation and convert it in an electric current that is then analyzed by a computer. In a typical experiment, the source will send radiation beam into the Michelson interferometer. Inside, a beam splitter will equally split the beam into two separate beams that reach the fixed and

the movable mirror. The beams are then reflected by the mirrors, causing an interference of the beams. The combined beam then reaches the sample, which absorbs a percentage of the radiation. The transmitted beam finally reaches the detector that converts the radiation to an electric current. The computer then produces an interferogram based on the amplitude of the generated volts depending on time. The Fourier transformation then transforms the interferogram from the time domain to the frequency domain, resulting in the intensity spectra of the sample.

References

[1] A. Mandal, R. Bisht, I. D. Rupenthal, and A. K. Mitra, "Polymeric micelles for ocular drug delivery: From structural frameworks to recent preclinical studies," *J. Control. Release*, vol. 248, pp. 96–116, 2017, doi: 10.1016/j.jconrel.2017.01.012.

[2] M. M. Lübtow, T. Lorson, T. Finger, F. K. Gröber-Becker, and R. Luxenhofer, "Combining Ultra-High Drug-Loaded Micelles and Injectable Hydrogel Drug Depots for Prolonged Drug Release," *Macromol. Chem. Phys.*, vol. 221, no. 1, 2020, doi: 10.1002/macp.201900341.

[3] C. Zhang, L. Liao, and S. Gong, "Microwave-assisted synthesis of PLLA-PEG-PLLA triblock copolymers," *Macromol. Rapid Commun.*, vol. 28, no. 4, pp. 422–427, 2007, doi: 10.1002/marc.200600709.

[4] Y. H. A. Hussein and M. Youssry, "Polymeric micelles of biodegradable diblock copolymers: Enhanced encapsulation of hydrophobic drugs," *Materials (Basel).*, vol. 11, no. 5, 2018, doi: 10.3390/ma11050688.

[5] K. K. Jain, "Drug delivery systems - An overview," *Methods Mol. Biol.*, vol. 437, pp. 1–50, 2008, doi: 10.1007/978-1-59745-210-6_1.

[6] S. S. Venkatraman, P. Jie, F. Min, B. Y. C. Freddy, and G. Leong-Huat, "Micelle-like nanoparticles of PLA-PEG-PLA triblock copolymer as chemotherapeutic carrier," *Int. J. Pharm.*, vol. 298, no. 1, pp. 219–232, 2005, doi: 10.1016/j.ijpharm.2005.03.023.

[7] C. H. Tsai, P. Y. Wang, I. C. Lin, H. Huang, G. S. Liu, and C. L. Tseng, "Ocular drug delivery: Role of degradable polymeric nanocarriers for ophthalmic application," *International Journal of Molecular Sciences*, vol. 19, no. 9. 2018, doi: 10.3390/ijms19092830.

[8] W. Gao, J. M. Chan, and O. C. Farokhzad, "PH-responsive nanoparticles for drug delivery," *Molecular Pharmaceutics*, vol. 7, no. 6. American Chemical Society, pp. 1913–1920, Dec. 06, 2010, doi: 10.1021/mp100253e.

[9] L. Zhang *et al.*, "Self-assembled lipid-polymer hybrid nanoparticles: A robust drug delivery platform," *ACS Nano*, vol. 2, no. 8, pp. 1696–1702, Aug. 2008, doi: 10.1021/nn800275r.

[10] E. M. del Amo, *Ocular and systemic pharmacokinetic models for drug*

discovery and development. 2015.

[11] A. Patel, "Ocular drug delivery systems: An overview," *World J. Pharmacol.*, vol. 2, no. 2, p. 47, 2013, doi: 10.5497/wjp.v2.i2.47.

[12] D. Lee, S. Cho, H. S. Park, and I. Kwon, "Ocular Drug Delivery through pHEMA-Hydrogel Contact Lenses Co-Loaded with Lipophilic Vitamins," *Sci. Reports 2016 61*, vol. 6, no. 1, pp. 1–8, Sep. 2016, doi: 10.1038/srep34194.

[13] J. Kim and A. Chauhan, "Dexamethasone transport and ocular delivery from poly(hydroxyethyl methacrylate) gels," *Int. J. Pharm.*, vol. 353, no. 1–2, pp. 205–222, Apr. 2008, doi: 10.1016/J.IJPHARM.2007.11.049.

[14] D. Gulsen, C. C. Li, and A. Chauhan, "Dispersion of DMPC Liposomes in Contact Lenses for Ophthalmic Drug Delivery," *http://dx.doi.org/10.1080/02713680500346633*, vol. 30, no. 12, pp. 1071–1080, Dec. 2009, doi: 10.1080/02713680500346633.

[15] S. S. Lee, P. Hughes, A. D. Ross, and M. R. Robinson, "Biodegradable implants for sustained drug release in the eye," *Pharm. Res.*, vol. 27, no. 10, pp. 2043–2053, Oct. 2010, doi: 10.1007/S11095-010-0159-X.

[16] R. F. Donnelly, T. R. Raj Singh, and A. D. Woolfson, "Microneedle-based drug delivery systems: Microfabrication, drug delivery, and safety," *Drug Deliv.*, vol. 17, no. 4, pp. 187–207, May 2010, doi: 10.3109/10717541003667798.

[17] J. Jiang, J. S. Moore, H. F. Edelhauser, and M. R. Prausnitz, "Intrascleral Drug Delivery to the Eye Using Hollow Microneedles," *Pharm. Res.*, vol. 26, no. 2, pp. 395–403, Feb. 2009, doi: 10.1007/s11095-008-9756-3.

[18] S. Liu, L. Jones, and F. X. Gu, "Nanomaterials for Ocular Drug Delivery," *Macromol. Biosci.*, vol. 12, no. 5, pp. 608–620, May 2012, doi: 10.1002/mabi.201100419.

[19] P. R. Karn, H. Do Kim, H. Kang, B. K. Sun, S. E. Jin, and S. J. Hwang, "Supercritical fluid-mediated liposomes containing cyclosporin A for the treatment of dry eye syndrome in a rabbit model: Comparative study with the conventional cyclosporin A emulsion," *Int. J. Nanomedicine*, 2014, doi: 10.2147/IJN.S65601.

[20] B. D. Ulery, L. S. Nair, and C. T. Laurencin, "Biomedical applications of biodegradable polymers," *Journal of Polymer Science, Part B: Polymer*

Physics. 2011, doi: 10.1002/polb.22259.

[21] H. K. Makadia and S. J. Siegel, "Poly Lactic-co-Glycolic Acid (PLGA) as biodegradable controlled drug delivery carrier," *Polymers (Basel).*, 2011, doi: 10.3390/polym3031377.

[22] M. S. Muthu, "Nanoparticles based on PLGA and its co-polymer: An overview," *Asian J. Pharm.*, vol. 3, no. 4, pp. 266–273, 2009, doi: 10.4103/0973-8398.59948.

[23] C. Cañadas *et al.*, "In vitro, ex vivo and in vivo characterization of PLGA nanoparticles loading pranoprofen for ocular administration," *Int. J. Pharm.*, 2016, doi: 10.1016/j.ijpharm.2016.07.055.

[24] K. Nagpal, S. K. Singh, and D. N. Mishra, "Chitosan nanoparticles: A promising system in novel drug delivery," *Chemical and Pharmaceutical Bulletin*. 2010, doi: 10.1248/cpb.58.1423.

[25] R. C. Nagarwal, P. N. Singh, S. Kant, P. Maiti, and J. K. Pandit, "Chitosan nanoparticles of 5-fluorouracil for ophthalmic delivery: Characterization, in-vitro and in-vivo study," *Chem. Pharm. Bull.*, 2011, doi: 10.1248/cpb.59.272.

[26] N. C. Silva, S. Silva, B. Sarmento, and M. Pintado, "Chitosan nanoparticles for daptomycin delivery in ocular treatment of bacterial endophthalmitis," *Drug Deliv.*, 2015, doi: 10.3109/10717544.2013.858195.

[27] S. Biswas, O. S. Vaze, S. Movassaghian, and V. P. Torchilin, "Polymeric Micelles for the Delivery of Poorly Soluble Drugs," *Drug Deliv. Strateg. Poorly Water-Soluble Drugs*, pp. 411–476, 2013, doi: 10.1002/9781118444726.ch14.

[28] D. A. Chiappetta and A. Sosnik, "Poly(ethylene oxide)-poly(propylene oxide) block copolymer micelles as drug delivery agents: Improved hydrosolubility, stability and bioavailability of drugs," *European Journal of Pharmaceutics and Biopharmaceutics*, vol. 66, no. 3. Elsevier, pp. 303–317, Jun. 01, 2007, doi: 10.1016/j.ejpb.2007.03.022.

[29] S. Fusco, A. Borzacchiello, and P. A. Netti, "Perspectives on: PEO-PPO-PEO Triblock Copolymers and their Biomedical Applications," *J. Bioact. Compat. Polym.*, vol. 21, no. 2, pp. 149–164, Mar. 2006, doi: 10.1177/0883911506063207.

[30] S. Y. Kim, I. G. Shin, Y. M. Lee, C. S. Cho, and Y. K. Sung, "Methoxy

poly(ethylene glycol) and ε-caprolactone amphiphilic block copolymeric micelle containing indomethacin. II. Micelle formation and drug release behaviours," *J. Control. Release*, vol. 51, no. 1, pp. 13–22, Jan. 1998, doi: 10.1016/S0168-3659(97)00124-7.

[31] C. Allen, Y. Yu, D. Maysinger, and A. Eisenberg, "Polycaprolactone-b-poly(ethylene oxide) block copolymer micelles as a novel drug delivery vehicle for neurotrophic agents FK506 and L-685,818," *Bioconjug. Chem.*, vol. 9, no. 5, pp. 564–572, Sep. 1998, doi: 10.1021/bc9702157.

[32] F. Chen, G. Yin, and X. Liao, "Preparation , characterization and in vitro release properties of morphine-loaded PLLA-PEG-PLLA microparticles via solution enhanced dispersion by supercritical fluids," pp. 1693–1705, 2013, doi: 10.1007/s10856-013-4926-1.

[33] X. Deng, S. Zhou, X. Li, J. Zhao, and M. Yuan, "In vitro degradation and release profiles for poly-dl-lactide-poly(ethylene glycol) microspheres containing human serum albumin," *J. Control. Release*, 2001, doi: 10.1016/S0168-3659(01)00210-3.

[34] H. Danafar, K. Rostamizadeh, S. Davaran, and M. Hamidi, "PLA-PEG-PLA copolymer-based polymersomes as nanocarriers for delivery of hydrophilic and hydrophobic drugs: Preparation and evaluation with atorvastatin and lisinopril," *Drug Dev. Ind. Pharm.*, vol. 40, no. 10, pp. 1411–1420, 2014, doi: 10.3109/03639045.2013.828223.

[35] C. Mu *et al.*, "Solubilization of flurbiprofen into aptamer-modified PEG-PLA micelles for targeted delivery to brain-derived endothelial cells in vitro," *J. Microencapsul.*, vol. 30, no. 7, pp. 701–708, 2013, doi: 10.3109/02652048.2013.778907.

[36] M. Imran, M. R. Shah, and Shafiullah, "Amphiphilic block copolymers–based micelles for drug delivery," in *Design and Development of New Nanocarriers*, Elsevier Inc., 2018, pp. 365–400.

[37] W. Zhou, C. Li, Z. Wang, W. Zhang, and J. Liu, "Factors affecting the stability of drug-loaded polymeric micelles and strategies for improvement," *J. Nanoparticle Res.*, vol. 18, no. 9, pp. 1–18, 2016, doi: 10.1007/s11051-016-3583-y.

[38] Y. Mai and A. Eisenberg, "Self-assembly of block copolymers," *Chem. Soc.*

Rev., vol. 41, no. 18, pp. 5969–5985, Aug. 2012, doi: 10.1039/c2cs35115c.

[39] S. C. Owen, D. P. Y. Chan, and M. S. Shoichet, "Polymeric micelle stability," *Nano Today*, vol. 7, pp. 53–65, 2012, doi: 10.1016/j.nantod.2012.01.002.

[40] K. E. Uhrich, S. M. Cannizzaro, R. S. Langer, and K. M. Shakesheff, "Polymeric Systems for Controlled Drug Release," *Chem. Rev.*, vol. 99, no. 11, pp. 3181–3198, 1999, doi: 10.1021/cr940351u.

[41] R. Z. Xiao, Z. W. Zeng, G. L. Zhou, J. J. Wang, F. Z. Li, and A. M. Wang, "Recent advances in PEG-PLA block copolymer nanoparticles," *Int. J. Nanomedicine*, vol. 5, no. 1, pp. 1057–1065, 2010, doi: 10.2147/IJN.S14912.

[42] T. Niwa, H. Takeuchi, T. Hino, N. Kunou, and Y. Kawashima, "Preparations of biodegradable nanospheres of water-soluble and insoluble drugs with D,L-lactide/glycolide copolymer by a novel spontaneous emulsification solvent diffusion method, and the drug release behavior," *J. Control. Release*, 1993, doi: 10.1016/0168-3659(93)90097-O.

[43] Z. L. Yang, R. L. Xin, W. Y. Ke, and Y. Liu, "Amphotericin B-loaded poly(ethylene glycol)-poly(lactide) micelles: Preparation, freeze-drying, and in vitro release," *J. Biomed. Mater. Res. - Part A*, 2008, doi: 10.1002/jbm.a.31504.

[44] Y. Luo, X. Yao, J. Yuan, T. Ding, and Q. Gao, "Preparation and drug controlled-release of polyion complex micelles as drug delivery systems," *Colloids Surfaces B Biointerfaces*, vol. 68, no. 2, pp. 218–224, Feb. 2009, doi: 10.1016/j.colsurfb.2008.10.014.

[45] Y. Wang, P. Li, T. T. D. Tran, J. Zhang, and L. Kong, "Manufacturing techniques and surface engineering of polymer based nanoparticles for targeted drug delivery to cancer," *Nanomaterials*, vol. 6, no. 2, 2016, doi: 10.3390/nano6020026.

[46] A. D. Jenkins, R. F. T. Stepto, P. Kratochvíl, and U. W. Suter, "Glossary of basic terms in polymer science (IUPAC Recommendations 1996)," *Pure Appl. Chem.*, vol. 68, no. 12, pp. 2287–2311, Jan. 1996, doi: 10.1351/pac199668122287.

[47] S. Metkar, V. Sathe, I. Rahman, B. Idage, and S. Idage, "Ring opening polymerization of lactide: kinetics and modeling," *Chem. Eng. Commun.*, vol. 206, no. 9, pp. 1159–1167, 2019, doi: 10.1080/00986445.2018.1550395.

[48] A. C. Albertsson and I. K. Varma, “Recent Developments in Ring Opening Polymerization of Lactones for Biomedical Applications,” *Biomacromolecules*, vol. 4, no. 6, pp. 1466–1486, Nov. 2003, doi: 10.1021/BM034247A.

[49] N. E. Kamber, W. Jeong, R. M. Waymouth, R. C. Pratt, B. G. G. Lohmeijer, and J. L. Hedrick, “Organocatalytic ring-opening polymerization,” *Chem. Rev.*, vol. 107, no. 12, pp. 5813–5840, 2007, doi: 10.1021/cr068415b.

[50] F. Ullah, M. B. H. Othman, F. Javed, Z. Ahmad, and H. M. Akil, “Classification, processing and application of hydrogels: A review,” *Mater. Sci. Eng. C*, vol. 57, pp. 414–433, Dec. 2015, doi: 10.1016/J.MSEC.2015.07.053.

[51] F. Abasalizadeh *et al.*, “Alginate-based hydrogels as drug delivery vehicles in cancer treatment and their applications in wound dressing and 3D bioprinting,” *J. Biol. Eng. 2020 141*, vol. 14, no. 1, pp. 1–22, Mar. 2020, doi: 10.1186/S13036-020-0227-7.

[52] S. V. Vinogradov, T. K. Bronich, and A. V. Kabanov, “Nanosized cationic hydrogels for drug delivery: preparation, properties and interactions with cells,” *Adv. Drug Deliv. Rev.*, vol. 54, no. 1, pp. 135–147, Jan. 2002, doi: 10.1016/S0169-409X(01)00245-9.

[53] M. Fathi-Achachelouei, D. Keskin, E. Bat, N. E. Vrana, and A. Tezcaner, “Dual growth factor delivery using PLGA nanoparticles in silk fibroin/PEGDMA hydrogels for articular cartilage tissue engineering,” *J. Biomed. Mater. Res. Part B Appl. Biomater.*, vol. 108, no. 5, pp. 2041–2062, Jul. 2020, doi: 10.1002/JBM.B.34544.

[54] Z. Li *et al.*, “A tough hydrogel-hydroxyapatite bone-like composite fabricated in situ by the electrophoresis approach,” *J. Mater. Chem. B*, vol. 1, no. 12, pp. 1755–1764, 2013, doi: 10.1039/c3tb00246b.

[55] S. Khan and N. M. Ranjha, “Effect of degree of cross-linking on swelling and on drug release of low viscous chitosan/poly(vinyl alcohol) hydrogels,” *Polym. Bull.*, vol. 71, no. 8, pp. 2133–2158, 2014, doi: 10.1007/s00289-014-1178-2.

[56] J. Li and D. J. Mooney, “Designing hydrogels for controlled drug delivery,” *Nat. Rev. Mater.*, vol. 1, no. 12, Oct. 2016, doi: 10.1038/NATREVMATS.2016.71.

[57] H. Nouailhas, A. El Ghzaoui, S. Li, and J. Coudane, “Stereocomplex-induced

gelation properties of polylactide/poly(ethylene glycol) diblock and triblock copolymers," *J. Appl. Polym. Sci.*, vol. 122, no. 3, pp. 1599–1606, Nov. 2011, doi: 10.1002/app.33896.

[58] G. Matijašić, M. Gretić, J. Vinčić, A. Poropat, L. Cuculić, and T. Rahelić, "Design and 3D printing of multi-compartmental PVA capsules for drug delivery," *J. Drug Deliv. Sci. Technol.*, vol. 52, pp. 677–686, Aug. 2019, doi: 10.1016/J.JDDST.2019.05.037.

[59] P. Li, Y. N. Dai, J. P. Zhang, A. Q. Wang, and Q. Wei, "Chitosan-Alginate Nanoparticles as a Novel Drug Delivery System for Nifedipine," *Int. J. Biomed. Sci.*, vol. 4, no. 3, p. 221, Sep. 2008, Accessed: Sep. 19, 2022. [Online]. Available: /pmc/articles/PMC3614711/.

[60] D. Olsen *et al.*, "Recombinant collagen and gelatin for drug delivery," *Adv. Drug Deliv. Rev.*, vol. 55, no. 12, pp. 1547–1567, Nov. 2003, doi: 10.1016/J.ADDR.2003.08.008.

[61] E. Esposito, E. Menegatti, and R. Cortesi, "Hyaluronan-based microspheres as tools for drug delivery: a comparative study," *Int. J. Pharm.*, vol. 288, no. 1, pp. 35–49, Jan. 2005, doi: 10.1016/J.IJPHARM.2004.09.001.

[62] V. G. Tacias-Pascacio *et al.*, "Dextran aldehyde in biocatalysis: More than a mere immobilization system," *Catalysts*, vol. 9, no. 7, 2019, doi: 10.3390/catal9070622.

[63] R. McCahon and J. Hardman, "Pharmacology of plasma expanders," *Anaesth. Intensive Care Med.*, vol. 18, no. 8, pp. 418–420, Aug. 2017, doi: 10.1016/j.mpaic.2017.05.005.

[64] J. F. Pan *et al.*, "One-step cross-linked injectable hydrogels with tunable properties for space-filling scaffolds in tissue engineering," *RSC Adv.*, vol. 5, no. 51, pp. 40820–40830, 2015, doi: 10.1039/c5ra02588e.

[65] J. Maia, R. A. Carvalho, J. F. J. Coelho, P. N. Simões, and M. H. Gil, "Insight on the periodate oxidation of dextran and its structural vicissitudes," *Polymer (Guildf).*, vol. 52, no. 2, pp. 258–265, 2011, doi: 10.1016/j.polymer.2010.11.058.

[66] M. F. Ishak and T. J. Painter, "Kinetic evidence for hemiacetal formation during the oxidation of dextran in aqueous periodate," *Carbohydr. Res.*, vol. 64, no. C, pp. 189–197, Jul. 1978, doi: 10.1016/S0008-6215(00)83700-3.

[67] W. Zhang, K. Zhang, S. Yan, J. Wu, and J. Yin, “A tough and self-healing poly(l -glutamic acid)-based composite hydrogel for tissue engineering,” *J. Mater. Chem. B*, vol. 6, no. 42, pp. 6865–6876, Oct. 2018, doi: 10.1039/C8TB01981A.

[68] S. J. Sonawane, R. S. Kalhapure, and T. Govender, “Hydrazone linkages in pH responsive drug delivery systems,” *Eur. J. Pharm. Sci.*, vol. 99, pp. 45–65, 2017, doi: 10.1016/j.ejps.2016.12.011.

[69] H. Tan, C. R. Chu, K. A. Payne, and K. G. Marra, “Injectable in situ forming biodegradable chitosan–hyaluronic acid based hydrogels for cartilage tissue engineering,” *Biomaterials*, vol. 30, no. 13, pp. 2499–2506, May 2009, doi: 10.1016/J.BIOMATERIALS.2008.12.080.

[70] S. Du *et al.*, “Covalent Chitosan-Cellulose Hydrogels via Schiff-Base Reaction Containing Macromolecular Microgels for pH-Sensitive Drug Delivery and Wound Dressing,” *Macromol. Chem. Phys.*, vol. 220, no. 23, p. 1900399, Dec. 2019, doi: 10.1002/MACP.201900399.

[71] N. Artzi, T. Shazly, C. Crespo, A. B. Ramos, H. K. Chenault, and E. R. Edelman, “Characterization of star adhesive sealants based on PEG/Dextran hydrogels,” *Macromol. Biosci.*, vol. 9, no. 8, pp. 754–765, 2009, doi: 10.1002/mabi.200800355.

[72] J. Simon *et al.*, “A fast method to measure the degree of oxidation of dialdehyde celluloses using multivariate calibration and infrared spectroscopy,” *Carbohydr. Polym.*, vol. 278, no. November 2021, p. 118887, 2022, doi: 10.1016/j.carbpol.2021.118887.

[73] S. Durmaz, S. Fank, and O. Okay, “Swelling and mechanical properties of solution-crosslinked poly(isobutylene) gels,” *Macromol. Chem. Phys.*, vol. 203, no. 4, pp. 663–672, 2002, doi: 10.1002/1521-3935(20020301)203:4<663::AID-MACP663>3.0.CO;2-W.